Error Estimates For A Partially Penalized Immersed Finite Element Method For Elasticity Interface Problems *

Ruchi Guo † Tao Lin ‡ Yanping Lin §

Abstract

This article is about the error analysis for a partially penalized immersed finite element (PPIFE) method designed to solve linear planar-elasticity problems whose Lamé parameters are piecewise constants with an interface-independent mesh. The bilinear form in this method contains penalties to handle the discontinuity in the global immersed finite element (IFE) functions across interface edges. We establish a stress trace inequality for IFE functions on interface elements, we employ a patch idea to derive an optimal error bound for the stress of the IFE interpolation on interface edges, and we design a suitable energy norm by which the bilinear form in this PPIFE method is coercive. These key ingredients enable us to prove that this PPIFE method converges optimally in both an energy norm and the usual L^2 norm under the standard piecewise H^2-regularity assumption for the exact solution. Features of the proposed PPIFE method are demonstrated with numerical examples.

1 Introduction

In this article, we discuss a partially penalized immersed finite element (PPIFE) method that uses an interface-independent mesh to solve the isotropic linear planar-elasticity interface problems:

$$-\operatorname{div}\sigma(\mathbf{u}) = \mathbf{f}, \quad \text{in } \Omega^- \cup \Omega^+, \tag{1.1a}$$
$$[\mathbf{u}]_\Gamma = \mathbf{0}, \quad \text{on } \Gamma, \tag{1.1b}$$
$$[\sigma(\mathbf{u})\mathbf{n}]_\Gamma = \mathbf{0}, \quad \text{on } \Gamma, \tag{1.1c}$$
$$\mathbf{u} = \mathbf{g}_D, \quad \text{on } \partial\Omega_D, \tag{1.1d}$$
$$\sigma(\mathbf{u})\mathbf{n} = \mathbf{g}_N \quad \text{on } \partial\Omega_N, \tag{1.1e}$$

where $\partial\Omega = \partial\Omega_D \cup \partial\Omega_N$ with $|\partial\Omega_D| \neq 0$, and $\sigma(\mathbf{u}) = (\sigma_{ij}(\mathbf{u}))_{1\leqslant i,j\leqslant 2}$ is the stress tensor given by

$$\sigma_{ij}(\mathbf{u}) = \lambda(\nabla\cdot\mathbf{u})\delta_{ij} + 2\mu\epsilon_{ij}(\mathbf{u}), \quad \text{with } \epsilon_{ij}(\mathbf{u}) = \frac{1}{2}\left(\frac{\partial u_i}{\partial x_j} + \frac{\partial u_j}{\partial x_i}\right) \tag{1.2}$$

being the strain tensor. Without loss of generality, we assume that the elastic object $\Omega \subset \mathbb{R}^2$ is a polygonal region whose edges are parallel to either the x-axis or the y-axis, and Ω is partitioned by a

*This research was partially supported by GRF 15301714/15327816 of HKSAR, and Polyu AMA-JRI

†Keywords: Interface problems, elasticity systems, discontinuous Lamé parameters, immersed finite element methods.

†Department of Mathematics, Virginia Tech, Blacksburg, VA 24061 (ruchi91@vt.edu)

‡Department of Mathematics, Virginia Tech, Blacksburg, VA 24061 (tlin@vt.edu)

§Department of Applied Mathematics, Hong Kong Polytechnic University, Kowloon, Hong Kong, China (yanping.lin@polyu.edu.hk)

smooth interface curve Γ into two subdomains Ω^- and Ω^+ occupied by different elastic materials such that the Lamé parameters are piecewise constants on Ω:

$$\lambda = \begin{cases} \lambda^- & \text{if } X = (x_1, x_2)^T \in \Omega^-, \\ \lambda^+ & \text{if } X = (x_1, x_2)^T \in \Omega^+, \end{cases} \qquad \mu = \begin{cases} \mu^- & \text{if } X = (x_1, x_2)^T \in \Omega^-, \\ \mu^+ & \text{if } X = (x_1, x_2)^T \in \Omega^+. \end{cases} \tag{1.3}$$

Traditional finite element methods or discontinuous Galerkin (DG) finite element methods require interface-fitted meshes to solve the elasticity system (1.1) with discontinuous Lamé parameters [13, 15, 29, 50]; otherwise, they might perform unsatisfactorily, see [5, 6, 11] for discussions about interface-fitted meshes for some interface problems. However, there are applications of elasticity interface problems that can benefit from numerical methods based on interface-independent meshes, for example, the shape optimization [45] and its applications in optimal design (elasticity compliance optimization) [2, 48] and inverse problems (elastography) [3, 32], to name just a few. In fact, in [23], the PPIFE method to be discussed has already been applied to an elastography type inverse problem through the shape optimization methodology such that large shape variations in the optimization can be handled accurately and efficiently on a fixed mesh. The goal of the present article is to establish a theoretical foundation for this PPIFE method with the linear or bilinear vector IFE spaces constructed in [21] on interface-independent meshes for solving the interface problems of the linear planar-elasticity system.

A fair number of studies have been carried out on developing numerical methods for solving the elasticity interface problems on interface-independent meshes. Among related literatures, two types of techniques are used in the finite element formulation around the interface to enforce the jump conditions. The first approach constructs suitable shape functions on elements around the interface according to the behaviors of the exact solutions so that they can produce good approximation, for example, the multiscale finite element method [12, 17], the extended finite element method [16, 46], and the partition of unity method [40, 47], as well as the immersed finite element (IFE) method to be discussed in this article. The other approach employs the standard polynomials as the shape functions but modifies the finite element weak formulation around the interface, such as the unfitted finite element methods [7, 27, 28]. Also, we refer readers to [4, 51, 52] for finite difference methods based a Cartesian mesh.

Among those methods based on interface-independent meshes, we think the IFE method and the unfitted finite element method have a closer relationship than to other methods in the sense that a finite element solution generated by either of these two methods is a standard polynomial when restricted on each non-interface element, but a macro polynomial (i.e., a piecewise polynomial) on each interface element defined according to the subelements partitioned by the interface curve. However, the IFE method and the unfitted finite element method use essentially different ways to patch two polynomials together to form the macro polynomial on each interface element. An unfitted finite element method uses two sets of polynomial shape functions on each interface element and uses a Nitsche's type penalty in the finite element scheme to glue them together according to the jump conditions. An IFE method employs one set of Hsieh-Clough-Tocher type [8, 14] macro shape functions on each interface element constructed to satisfy the jump conditions in an approximate sense, i.e., the IFE shape function on each interface element satisfy interface jump conditions approximately on a line segment determined by the interface inside the interface element. This essential difference leads to different degrees of freedom around the interface for these two methods. Both the total number and location of degrees of freedom of an IFE space are fixed and independent of the interface, and an IFE space is actually isomorphic to the standard H^1-conforming finite element space defined on the same mesh. Hence the size and algebraic structure of the resulted linear system keep unchanged regardless of the interface shape and location on a chosen fixed mesh. This feature of IFE methods can benefit some applications especially those involving moving interface and the related implementation, for example, the method of lines [42] can be readily adopted for using an IFE method to solve problems with a moving interface [31, 37], and the shape optimization methodology can

naturally work together with IFE methods to solve some interface inverse problems so that the numerical interface can be adjusted in the optimization procedure on a fixed mesh [22, 23].

On the other hand, the need to use IFE shape functions instead of just using generic FE polynomials does make the application of an IFE method slightly more complicated than unfitted finite element methods. Basically, one needs to create and implement IFE shape functions as well as the local IFE matrix and vector assembling programs to be used on interface elements. Nevertheless, the implementation of the local IFE matrix and vector assembling programs on an interface element follows the same procedure as their FE counterparts except that the involved integrals have to be computed on subelements because IFE shape functions are piecewisely defined. We also note that standard local FE matrix and vector assembling programs are employed on most of the elements in a mesh for an IFE method because interface elements form a small subset in a mesh fine enough.

Like all IFE spaces available in the literature, the IFE space to be used in the present article is also discontinuous across interface edges in a mesh [1, 18, 21]. To reduce the adverse effects from this discontinuity, we follow the idea of [38] to apply suitable penalties (interior penalities) at all interface edges in a so called partially penalized IFE (PPIFE) method, which, in a certain sense, can be considered as an extension of the one in [38] for scalar elliptic interface problems to interface problems of an elliptic system. A similar idea of using penalties to handle the discontinuities of basis functions is also employed in [19, 26, 33], but the penalties in these articles are added on both interface edges and non-interface edges of interface elements since their basis functions may not be continuous across those two types of edges. The local IFE functions in this article are determined by the Lagrange type degrees of freedom at mesh nodes [21] such that they are used to form the global IFE functions continuous at mesh nodes, and consequently, the IFE functions are continuous across all the non-interface edges. This continuity allows us to use penalties only on interface edges. We note that the ghost penalties [9], i.e., the higher-order penalties, are also employed around the interface to enhance the robustness for some unfitted mesh methods, we refer readers to [10] and [7] for more discussions about this penalty technique applied to the scalar elliptic interface problems and elasticity interface problems, respectively.

The contributions of the present article include two fundamental estimates. The first is a trace inequality on interface elements for the stress of the elasticity IFE functions in the vector form in which the constant in the bound is independent of the interface location. Trace inequalities on interface elements are important tools in the error analysis of unfitted mesh methods. For example, a special trace inequality for penalties on interface with certain weights depending on the measure of subelements has been developed for showing stability in the unfitted finite element method [7, 27, 28]. The second estimate is about the optimal approximation capabilities of the vector IFE space for elasticity in terms of a specially designed energy norm involving the stress on interface edges. An estimate for the flux of the IFE interpolation is established in [38] for the scalar IFE space with an excessive H^3-regularity assumption, and we seek new techniques based on the patch element idea [25, 26] to avoid this strong regularity assumption. More importantly, these fundamental estimates enable us to show that the proposed PPIFE method can converge optimally in the energy norm and in the usual L^2 norm under the standard piecewise H^2-regularity assumption for the exact solution. To our best knowledge, this is the first IFE method for the planar-elasticity interface problems whose optimal error bounds have been theoretically proved.

The vector IFE functions employed in this article are based on a unified construction framework through a Sherman-Morrison system [18, 21] which is advantages for implementation since the structure of their formulas does not depend on how the interface cuts each element. Recently, this construction framework has been extended to the construction of IFE functions for solving the scalar elliptic interface problems [20] in three-dimensional space. We therefore believe that the proposed PPIFE scheme based on the vector IFE functions in [21] is readily extendable to the 3-D elasticity interface problems, but of course, the related analysis in three-dimensional space is more challenging, and we hope the work presented in this article can shed light on both the development and analysis of IFE methods for 3-D

elasticity interface problems.

This article is organized as follows. In the next section, we introduce some basic notations and describe the PPIFE method for the elasticity interface problems (1.1). In Section 3, we establish a stress trace inequality for the elasticity IFE functions. In Section 4, we show an optimal error bound on interface edges for the IFE interpolation, and then prove the optimal approximation capability of the IFE space in terms of an energy norm. In Section 5, we show that the bilinear form in this PPIFE method is both coercive and bounded, and these results facilitate the proof of the fact that the PPIFE solution converges to the exact solution optimally in the energy norm and L^2 norm. In the last section, we present numerical examples to demonstrate features of this PPIFE method.

2 Notations And The PPIFE Method

In this section, we first introduce a few basic notations to be used in this article. We recall the IFE spaces based on linear and bilinear polynomials, respectively, for the linear elasticity interface problems. We then describe the PPIFE method that uses these IFE spaces to solve the elasticity interface problems with interface-independent meshes.

2.1 Some Basic Notations

Throughout this article, on every measurable subset $\widetilde{\Omega} \subseteq \Omega$, we denote the standard Sobolev space by $W^{k,p}(\widetilde{\Omega})$ with the norms $\|\cdot\|_{W^{k,p}(\widetilde{\Omega})}$, $k \geqslant 1$, $1 \leqslant p < \infty$. For any tensor $\mathbf{w} = (w_{ij})_{i,j=1}^{m,n} \in \left[W^{k,p}(\widetilde{\Omega})\right]^{m\times n}$, we define the associated norm as

$$\|\mathbf{w}\|_{W^{k,p}(\widetilde{\Omega})} = \sum_{i,j=1}^{m,n} \|w_{ij}\|_{W^{k,p}(\widetilde{\Omega})}. \tag{2.1}$$

In the case $\widetilde{\Omega} \cap \Gamma \neq \emptyset$, we let $\widetilde{\Omega}^s = \widetilde{\Omega} \cap \Omega^s$, $s = \pm$, and introduce a split Sobolev space and the associated norms

$$\mathbf{PW}^{k,p}(\widetilde{\Omega}) = \left\{\mathbf{v} \in \left[W^{1,p}(\widetilde{\Omega})\right]^2 : \mathbf{v}|_{\widetilde{\Omega}^s} \in \left[W^{k,p}(\widetilde{\Omega}^s)\right]^2,\ s = \pm;\ [\mathbf{v}]_\Gamma = \mathbf{0},\ \text{and } [\sigma(\mathbf{v})\mathbf{n}]_\Gamma = \mathbf{0}\right\}, \tag{2.2a}$$

$$\|\mathbf{v}\|_{\mathbf{PW}^{k,p}(\widetilde{\Omega})} = \|\mathbf{v}\|_{\mathbf{PW}^{k,p}(\widetilde{\Omega}^-)} + \|\mathbf{v}\|_{\mathbf{PW}^{k,p}(\widetilde{\Omega}^+)}. \tag{2.2b}$$

We note that for every $\mathbf{v} \in \mathbf{PW}^{k,p}(\widetilde{\Omega})$, the definition above implicitly requires that the 0-th and 1st traces of $\mathbf{v}$ are well defined on Γ. In particular, if $p = 2$, we have the Hilbert spaces $H^k(\widetilde{\Omega})$ and $\mathbf{PH}^k(\widetilde{\Omega})$ with the norms $\|\cdot\|_{H^k(\widetilde{\Omega})}$ and $\|\cdot\|_{\mathbf{PH}^k(\widetilde{\Omega})}$, respectively. In our analysis, we assume that the exact solution $\mathbf{u}$ to the interface problem (1.1a)-(1.1e) has a piecewise H^2 regularity, i.e., $\mathbf{u} \in \mathbf{PH}^2(\Omega)$. This assumption can be satisfied under certain conditions on the interface, and a related regularity analysis can be found in [34, 41].

To facilitate a clear presentation of the main ideas in our analysis, we follow the tradition to discuss only the interface problem with a homogeneous boundary condition, i.e. $\mathbf{g}_D = \mathbf{0}$ on $\partial\Omega_D$ and $\mathbf{g}_N = \mathbf{0}$ on $\partial\Omega_N$, and we assume the interface does not meet the boundary. The IFE methods and their related error analysis to be presented are readily extendable to handle more general cases.

In this article, we consider an interface independent Cartesian triangular or rectangular mesh $\mathcal{T}_h$ of Ω, and we use $\mathcal{N}_h$ and $\mathcal{E}_h$ to denote the collections of its nodes and edges, respectively. An element is called an interface element if its interior has non-empty intersection with the interface; otherwise, it is called a non-interface element. For example, if an element has some edge exactly matching a linear portion of

an interface but its interior has empty intersection with the interface, then it is still considered as a non-interface element in the proposed IFE method. Also, if an element has some edge partially matching the interface and its interior also intersects the interface, then it is an interface element but only the portion of the interface inside the element will be considered for this interface element. By this description of an interface element, following [18, 30, 35] with suitable rotations and without loss of generality, we can assume that, when the mesh is sufficiently fine, i.e., the interface is locally flat enough inside each interface element, there are only two possible interface element configurations shown in Figures 2.1 and 2.2 for rectangular and triangular elements, respectively. Furthermore, in this mesh, we let $\mathcal{T}_h^i(\mathcal{E}_h^i)$ and $\mathcal{T}_h^n(\mathcal{E}_h^n)$ be the sets of interface and non-interface elements (edges), respectively. We also denote the set of interior interface edges by $\mathring{\mathcal{E}}_h^i$, let $\mathring{\mathcal{E}}_h^n$ be the set of interior non-interface edges, and we obviously have $\mathring{\mathcal{E}}_h = \mathring{\mathcal{E}}_h^i \cup \mathring{\mathcal{E}}_h^n$, here $\mathring{\mathcal{E}}_h$ is the set of interior edges of the mesh.

With the mesh $\mathcal{T}_h$, we introduce the following space

$$\begin{aligned}\mathbf{V}_h = \Big\{ \mathbf{v} : \mathbf{v}|_T \in \left[H^1(T)\right]^2,\ \forall T \in \mathcal{T}_h,\ \mathbf{v} \text{ is continuous at each } N \in \mathcal{N}_h, \\ \mathbf{v} \text{ is continuous across each } e \in \mathring{\mathcal{E}}_h^n,\ \mathbf{v}|_{\partial\Omega_D} = \mathbf{0} \Big\}.\end{aligned} \tag{2.3}$$

On every $e \in \mathring{\mathcal{E}}_h$ shared by two elements T_e^1 and T_e^2, we adopt the following standard notations for the average and jump over e for every $\mathbf{g} \in \mathbf{V}_h$:

$$\{\mathbf{g}\}_e = \frac{(\mathbf{g}|_{T_e^1})|_e + (\mathbf{g}|_{T_e^2})|_e}{2}, \quad \text{and} \quad [\mathbf{g}]_e = (\mathbf{g}|_{T_e^1})|_e - (\mathbf{g}|_{T_e^2})|_e. \tag{2.4}$$

For the simplicity of presentation, we may drop e if there is no danger of causing any confusion.

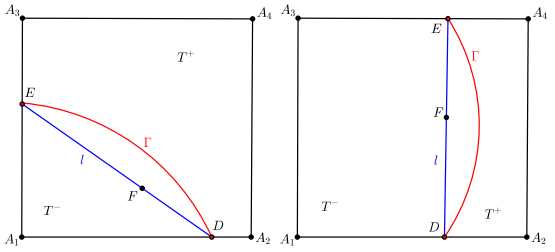

(a) Type 1 (b) Type 2

Figure 2.1: Rectangular (bilinear) elements

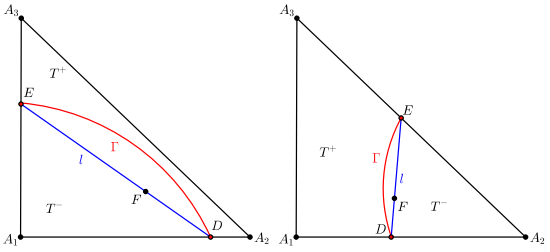

(a) Type 1 (b) Type 2

Figure 2.2: Triangular (linear) elements

2.2 IFE Spaces And The PPIFE Method

In this section, we first recall the linear and bilinear IFE spaces developed in [21] for the linear elasticity interface problems. Then we present the PPIFE method for solving elasticity interface problems. For each element $T \in \mathcal{T}_h$, according to whether T is triangular or rectangular, we let $\Pi_T = [\mathbb{P}_1(T)]^2$ or $[\mathbb{Q}_1(T)]^2$, and let $\mathcal{I}_T = \{1, 2, 3\}$ or $\mathcal{I}_T = \{1, 2, 3, 4\}$. On each interface element $T \in \mathcal{T}_h^i$, we let l be the line segment determined by the intersection points D and E of the interface and ∂T, see Figures 2.1 and 2.2 for illustrations. Let $\bar{\mathbf{n}} = (\bar{n}_1, \bar{n}_2)^T$ and $\bar{\mathbf{t}} = (\bar{n}_2, -\bar{n}_1)^T$ be the normal vector and tangential vector to l. Then $L(X) = 0$ with $L(X) = (X - D) \cdot \bar{\mathbf{n}}$ is the equation for the line passing l. Without causing any confusion, we let l partition T into T^- and T^+. On T, recall the elasticity IFE functions [21] as piecewise vector linear or bilinear polynomials in the following format:

$$\boldsymbol{\phi}_T(X) = \begin{cases} \boldsymbol{\phi}_T^-(X) \in \boldsymbol{\Pi}_T, & \text{if } X \in T^-, \\ \boldsymbol{\phi}_T^+(X) \in \boldsymbol{\Pi}_T, & \text{if } X \in T^+, \end{cases} \tag{2.5}$$

with $\boldsymbol{\phi}_T^+(X)$ and $\boldsymbol{\phi}_T^-(X)$ satisfying approximate jump conditions

$$\begin{cases} \boldsymbol{\phi}_T^-|_l = \boldsymbol{\phi}_T^+|_l, & \text{(for the linear case)}, \\ \boldsymbol{\phi}_T^-|_l = \boldsymbol{\phi}_T^+|_l, \quad d(\boldsymbol{\phi}_T^-) = d(\boldsymbol{\phi}_T^+), & \text{(for the bilinear } Q_1 \text{ case)}, \end{cases} \tag{2.6}$$

$$\sigma^+(\boldsymbol{\phi}_T^+)(F)\ \bar{\mathbf{n}} = \sigma^-(\boldsymbol{\phi}_T^-)(F)\ \bar{\mathbf{n}}, \tag{2.7}$$

where F is a point on l specified in [21] and $d(\boldsymbol{\psi})$ is a vector formed by the coefficients of the second degree term xy in a vector bilinear polynomial $\boldsymbol{\psi}$. According to Theorem 5.1 and Remark 5.3 in [21], there is a unique IFE function $\boldsymbol{\phi}_{i,T}$ that satisfies (2.5)-(2.7) and

$$\boldsymbol{\phi}_{i,T}(A_j) = \begin{bmatrix} \delta_{i,j} \\ 0 \end{bmatrix},\ i = 1, \cdots, |\mathcal{I}_T|, \quad \text{or} \quad \boldsymbol{\phi}_{i,T}(A_j) = \begin{bmatrix} 0, \\ \delta_{i-|\mathcal{I}_T|,j}, \end{bmatrix},\ \ i = |\mathcal{I}_T|+1, \cdots, 2|\mathcal{I}_T|. \tag{2.8}$$

It is easy to verify that these IFE functions are linearly independent; hence, we call them the IFE shape functions on the interface element T, and we use them to define the local IFE spaces on each $T \in \mathcal{T}_h^i$ as follows:

$$\mathbf{S}_h(T) = \text{Span}\{\boldsymbol{\phi}_{i,T} : 1 \leqslant i \leqslant 2|\mathcal{I}_T|\}. \tag{2.9}$$

On each non-interface element $T \in \mathcal{T}_h^n$, we simply let the local IFE space be $\mathbf{S}_h(T) = \mathbf{\Pi}_T$ and adopt the standard local Lagrange vector shape functions on T as the IFE shape functions. Similar to [38], the global IFE space is then constructed by enforcing the continuity at nodes:

$$\mathbf{S}_h(\Omega) = \big\{\mathbf{v} : \mathbf{v}|_T \in \mathbf{S}_h(T),\ \forall T \in \mathcal{T}_h;\ \mathbf{v} \text{ is continuous at each } N \in \mathcal{N}_h;\ \mathbf{v}|_{\partial\Omega_D} = \mathbf{0}\big\}. \tag{2.10}$$

We highlight that the degrees of freedom for the local IFE space $S_h(T)$ is $2|\mathcal{I}_T|$ which is the same as the standard local finite element space, and on a given mesh, the degrees of freedom of the global IFE space $\mathbf{S}_h(\Omega)$ is also the same as the usual H^1 finite element space constructed with linear or bilinear polynomials. Furthermore, we note that $\mathbf{S}_h(\Omega) \subset \mathbf{V}_h$, but $\mathbf{S}_h(\Omega) \subset H^1(\Omega \backslash (\cup_{T\in\mathcal{T}_h^i} T))$ because an IFE function in $\mathbf{S}_h(\Omega)$ can be discontinuous across an interface edges $e \in \mathring{\mathcal{E}}_h^i$, and this discontinuity leads to challenges to the error analysis of the IFE method to be described.

Now, we describe the PPIFE scheme for the elasticity interface problem (1.1a)-(1.1e). As usual, by the Green's formula, we have

$$-\int_T (\text{div } \sigma(\mathbf{u})) \cdot \mathbf{v} dX = \int_T \nabla\mathbf{v} : \sigma(\mathbf{u}) dX - \int_{\partial T} (\sigma(\mathbf{u})\mathbf{n}) \cdot \mathbf{v} ds, \quad \forall \mathbf{v} \in \mathbf{V}_h,\ \ \forall T \in \mathcal{T}_h, \tag{2.11}$$

where $\nabla = (\partial_{x_1}, \partial_{x_2})$ is the gradient operator as a row vector. Then, summing (2.11) over all the elements and using the continuity of $\mathbf{v} \in \mathbf{V}_h$ on all the non-interface edges $e \in \mathring{\mathcal{E}}_h^n$, we have

$$\sum_{T\in\mathcal{T}_h} \int_T \nabla\mathbf{v} : \sigma(\mathbf{u}) dX - \sum_{e\in\mathring{\mathcal{E}}_h^i} \int_e \{\sigma(\mathbf{u})\mathbf{n}_e\} \cdot [\mathbf{v}] ds = \int_\Omega \mathbf{f} \cdot \mathbf{v} dX, \tag{2.12}$$

where $\mathbf{n}_e$ is from T_e^1 to T_e^2 which are the two elements sharing the edge e. The regularity assumption for $\mathbf{u}$ satisfying (1.1a)-(1.1e) yields the continuity across all the edges, and thus

$$\int_e \{\sigma(\mathbf{v})\mathbf{n}_e\} \cdot [\mathbf{u}] ds = 0, \quad \text{and} \quad \int_e [\mathbf{u}] \cdot [\mathbf{v}] ds = 0, \ \ \forall e \in \mathring{\mathcal{E}}_h^i. \tag{2.13}$$

Adding these vanishing terms in (2.13) to (2.12) leads to a weak form for (1.1a)-(1.1e):

$$a_h(\mathbf{u}, \mathbf{v}) = L_f(\mathbf{v}), \quad \forall \mathbf{v} \in \mathbf{V}_h, \tag{2.14}$$

$$\text{where} \quad a_h(\mathbf{u},\mathbf{v}) = \sum_{T\in\mathcal{T}_h}\int_T 2\mu\epsilon(\mathbf{u}):\epsilon(\mathbf{v})dX + \sum_{T\in\mathcal{T}_h}\int_T \lambda(\nabla\cdot\mathbf{u})(\nabla\cdot\mathbf{v})dX$$
$$- \sum_{e\in\mathring{\mathcal{E}}_h^i}\int_e \{\sigma(\mathbf{u})\mathbf{n}_e\}\cdot[\mathbf{v}]ds + \theta\sum_{e\in\mathring{\mathcal{E}}_h^i}\int_e \{\sigma(\mathbf{v})\mathbf{n}_e\}\cdot[\mathbf{u}]ds + \sum_{e\in\mathring{\mathcal{E}}_h^i}\frac{\rho}{h}\int_e [\mathbf{u}]\cdot[\mathbf{v}]ds, \tag{2.15}$$
$$\text{and} \quad L_f(\mathbf{v}) = \sum_{T\in\mathcal{T}_h}\int_T \mathbf{f}\cdot\mathbf{v}dX, \tag{2.16}$$

and ρ is a stabilizing parameter for the scheme. According to the weak form (2.14) and the fact the IFE space $\mathbf{S}_h(\Omega)$ is a subspace of $\mathbf{V}_h$ with the optimal approximation capability [21], we consider the IFE method for the isotropic planar-elasticity interface problem (1.1) as finding $\mathbf{u}_h \in \mathbf{S}_h(\Omega)$ such that

$$a_h(\mathbf{u}_h,\mathbf{v}_h) = L_f(\mathbf{v}_h), \quad \forall \mathbf{v}_h \in \mathbf{S}_h(\Omega). \tag{2.17}$$

We note that the bilinear form in (2.15) contains penalties imposed only on the interface edges, and this feature suggests us to call this IFE method the partially penalized IFE (PPIFE) method. We highlight that not only the location but also the purpose of the penalties are different from those in the unfitted finite element method [7, 15, 27, 28]. The PPIFE method uses these penalties to alleviate the adverse effects of the discontinuities in IFE functions on interface edges, while the unfitted finite element method employs the penalties on the interface to enforce the jump conditions. For the PPIFE method, we emphasize that the jump conditions have already been enforced in the IFE functions themselves by (2.6) and (2.7).

In this article, we will consider the PPIFE schemes associated with the three popular choices for the parameter: $\theta = -1, 0, 1$, and following the convention in the literature [38, 44], we call the corresponding PPIFE method the symmetric, incomplete, and non-symmetric PPIFE (SPPIFE, IPPIFE and NPPIFE) methods, respectively.

3 A Trace Inequality For Vector IFE Functions

In this section, we derive a trace inequality for the elasticity IFE functions on each interface element $T \in \mathcal{T}_h^i$. According to the description in Section 2.1, with suitable rotations, there are only two interface configurations for both the rectangular and triangular interface elements, see Figures 2.1 and 2.2. Without loss of generality, the rest of our discussions in this section are all based on the interface element configurations in Figures 2.1 and 2.2.

We recall from [21] that, for each local elasticity IFE function $\boldsymbol{\phi}_T$ specified by (2.5)-(2.7), its two component polynomials $\boldsymbol{\phi}_T^{\pm} \in \boldsymbol{\Pi}_T$ are related with each other according to

$$\boldsymbol{\phi}_T^- - \boldsymbol{\phi}_T^+ = \mathbf{c}_0 L(X), \tag{3.1}$$

with the coefficient vector $\mathbf{c}_0$ expressed as

$$\mathbf{c}_0 = \left(K^-\right)^{-1}\hat{\sigma}(\boldsymbol{\phi}_T^+)(F)\bar{\mathbf{n}}, \tag{3.2a}$$
$$\text{with} \quad K^s = Q\mathcal{P}^s Q^T \quad \text{and} \quad Q = [\bar{\mathbf{n}},\bar{\mathbf{t}}], \quad \mathcal{P}^s = \begin{bmatrix} \lambda^s + 2\mu^s & 0 \\ 0 & \mu^s \end{bmatrix}, \quad s = \pm, \tag{3.2b}$$

where F is the same point in (2.7), and $\hat{\sigma}(\mathbf{v}) = (\hat{\sigma}_{ij}(\mathbf{v}))_{1\leqslant i,j\leqslant 2}$ for every $\mathbf{v} \in \left[H^1(T)\right]^2$ in which $\hat{\sigma}_{ij}$ is defined according to (1.2) but with the λ and μ replaced by $\hat{\lambda} = \lambda^+ - \lambda^-$ and $\hat{\mu} = \mu^+ - \mu^-$.

Since IFE functions are macro polynomials (piecewise polynomials) in the format given in (2.5) which are not in $\left[H^2(T)\right]^2$ for an interface element T in general, the first order trace inequality commonly used

in error estimation for finite element methods can not be applied to IFE functions on the whole element T directly. Nevertheless, an IFE function $\boldsymbol{\phi}_T$ in the macro polynomial format of (2.5) is in fact somewhat close to a simple polynomial in the sense that its two component polynomials $\boldsymbol{\phi}_T^{\pm} \in \boldsymbol{\Pi}_T$ are closely related to each other by (3.1), and this suggests a possibility for us to derive a first order trace inequality for IFE functions used in the present article.

We start from recalling the following trace inequalities for polynomials [49]:

$$\forall v \in \mathbb{P}_k(m), \quad \forall t \in \partial m, \quad |v(t)| \leqslant \frac{k+1}{\sqrt{|m|}} \|v\|_{L^2(m)}, \quad \text{for a 1-d segment } m; \tag{3.3}$$

$$\forall v \in \mathbb{P}_k(T), \quad \forall e \text{ be an edge of } T, \quad \|v\|_{L^2(e)} \leqslant \sqrt{\frac{(k+1)(k+2)}{2} \frac{|e|}{|T|}} \|v\|_{L^2(T)}, \quad \text{for a 2-d triangle } T. \tag{3.4}$$

First, we establish a few estimates about $\mathbf{c}_0 L(X)$ which, according to (3.1) and the discussion above, is a key for deriving the special trace inequality for IFE functions needed in the error analysis. We note that $\sigma^-(\mathbf{c}_0 L)$ is a constant matrix independent of the spatial variable X.

Lemma 3.1. *There exists a constant C independent of the interface location and Lamé parameters such that*

$$\|\sigma^-(\mathbf{c}_0 L)\| \leqslant \frac{C}{|l|^{1/2}} \|\hat{\sigma}(\boldsymbol{\phi}_T^+)\bar{\mathbf{n}}\|_{L^2(l)}. \tag{3.5}$$

Proof. Let $\mathbf{c}_0 = (c_0^1, c_0^2)^T$. Using the formula $L(X) = \bar{\mathbf{n}} \cdot (X - D)$ with $\bar{\mathbf{n}} = (\bar{n}_1, \bar{n}_2)^T$, we have

$$\sigma^-(\mathbf{c}_0 L) = \begin{bmatrix} (\lambda^- + 2\mu^-)c_0^1 \bar{n}_1 + \lambda^- c_0^2 \bar{n}_2 & \mu^-(c_0^1 \bar{n}_2 + c_0^2 \bar{n}_1) \\ \mu^-(c_0^1 \bar{n}_2 + c_0^2 \bar{n}_1) & (\lambda^- + 2\mu^-)c_0^2 \bar{n}_2 + \lambda^- c_0^1 \bar{n}_1 \end{bmatrix}. \tag{3.6}$$

Given any unit vector $\mathbf{r} = (r_1, r_2)^T$, using (3.2a) and (3.6), we obtain

$$\sigma^-(\mathbf{c}_0 L)\mathbf{r} = \begin{bmatrix} \lambda^- r_1 + 2\mu^- \bar{n}_1 \mathbf{r} \cdot \bar{\mathbf{n}} & \mu^-(2\bar{n}_1 \bar{n}_2 r_1 + \bar{n}_2^2 r_2 - \bar{n}_1^2 r_2) \\ \lambda^- r_2 + 2\mu^- \bar{n}_2 \mathbf{r} \cdot \bar{\mathbf{n}} & -\mu^-(2\bar{n}_1 \bar{n}_2 r_2 + \bar{n}_1^2 r_1 - \bar{n}_2^2 r_1) \end{bmatrix} (\mathcal{P}^-)^{-1} Q^T \hat{\sigma}(\boldsymbol{\phi}_T^+)(F)\bar{\mathbf{n}}. \tag{3.7}$$

Rewrite (3.7) as $\sigma^-(\mathbf{c}_0 L)\mathbf{r} = \Lambda(\mathbf{r})\hat{\sigma}(\boldsymbol{\phi}_T^+)(F)\bar{\mathbf{n}}$. Then, taking $\mathbf{r} = \bar{\mathbf{n}}$, $\bar{\mathbf{t}}$, we have

$$\Lambda(\bar{\mathbf{n}}) = I_2, \quad \text{and} \quad \Lambda(\bar{\mathbf{t}}) = \begin{bmatrix} \frac{\lambda^-}{\lambda^- + 2\mu^-} \bar{n}_2 & \bar{n}_1 \\ \frac{-\lambda^-}{\lambda^- + 2\mu^-} \bar{n}_1 & \bar{n}_2 \end{bmatrix} Q^T, \tag{3.8}$$

where I_2 is the 2-by-2 identity matrix. Hence, we have $\|\sigma^-(\mathbf{c}_0 L)\bar{\mathbf{n}}\| = \|\hat{\sigma}(\boldsymbol{\phi}_T^+)(F)\bar{\mathbf{n}}\|$, and a direct computation yields

$$\begin{aligned} \|\sigma^-(\mathbf{c}_0 L)\bar{\mathbf{t}}\| &\leqslant \|\Lambda(\bar{\mathbf{t}})\|_F \|\hat{\sigma}(\boldsymbol{\phi}_T^+)(F)\bar{\mathbf{n}}\| \\ &= \sqrt{\left(1 + \frac{(\lambda^-)^2}{(\lambda^- + 2\mu^-)^2}\right)\left(1 + 2\bar{n}_1^2 \bar{n}_2^2\right)} \|\hat{\sigma}(\boldsymbol{\phi}_T^+)(F)\bar{\mathbf{n}}\| \\ &\leqslant \sqrt{3} \|\hat{\sigma}(\boldsymbol{\phi}_T^+)(F)\bar{\mathbf{n}}\|, \end{aligned} \tag{3.9}$$

where $\|\cdot\|_F$ denotes the Frobenius norm. Therefore, for every unit vector $\mathbf{r}$, we have

$$\|\sigma^-(\mathbf{c}_0 L)\mathbf{r}\| \leqslant \left(\|\sigma^-(\mathbf{c}_0 L)\bar{\mathbf{n}}\|^2 + \|\sigma^-(\mathbf{c}_0 L)\bar{\mathbf{t}}\|^2\right)^{1/2} \leqslant 2\|\hat{\sigma}(\boldsymbol{\phi}_T^+)(F)\bar{\mathbf{n}}\|. \tag{3.10}$$

Using (3.10) with $\mathbf{r} = \mathbf{e}_1$ and $\mathbf{e}_2$ where $\mathbf{e}_i$ is the i-th unit vector in $\mathbb{R}^2$, we obtain

$$\|\sigma^-(\mathbf{c}_0 L)\| \leqslant \|\sigma^-(\mathbf{c}_0 L)\mathbf{e}_1\| + \|\sigma^-(\mathbf{c}_0 L)\mathbf{e}_2\| \leqslant 4\|\hat{\sigma}(\boldsymbol{\phi}_T^+)(F)\bar{\mathbf{n}}\|. \tag{3.11}$$

In addition, on the line l, without loss of generality, we can assume $\left|\overline{DF}\right| \geqslant |l|/2$. Then, applying the standard 1-D trace inequality (3.3) to (3.11) with $m = \overline{DF}$, we obtain (3.5). □

As discussed in the following lemma, the estimate given by (3.5) can be refined so that its bound is expressed in terms of the IFE function $\boldsymbol{\phi}_T(X)$ and the ratios of the Lamé parameters in the two subelements of $T \in \mathcal{T}_h^i$. We denote $\lambda_M = \max\{\lambda^+, \lambda^-\}$, $\lambda_m = \min\{\lambda^+, \lambda^-\}$ and define μ_M and μ_m similarly.

Lemma 3.2. *There exists a constant C independent of the interface location and Lamé parameters such that*

$$\|\sigma^-(\mathbf{c}_0 L)\| \leqslant \frac{C}{h^{1/2}|l|^{1/2}} \left(\frac{\mu_M}{\sqrt{\mu_m}} \|\sqrt{2\mu}\epsilon(\boldsymbol{\phi}_T)\|_{L^2(T)} + \frac{\lambda_M}{\sqrt{\lambda_m}} \|\sqrt{\lambda}\nabla \cdot \boldsymbol{\phi}_T\|_{L^2(T)} \right) \tag{3.12}$$

for every IFE function $\boldsymbol{\phi}_T$ on an interface element T satisfying one of the following conditions:

(a): T is a Type 1 rectangular interface element illustrated in Figure 2.1.

(b): T is a Type 1 triangular interface element illustrated in Figure 2.2 such that $|A_1D| \leqslant h/2$ or $|A_1E| \leqslant h/2$.

(c): T is a Type 2 triangular interface element illustrated in Figure 2.2 such that $|A_2D| \leqslant h/2$ or $|A_2E| \leqslant h/2$.

Proof. Assume T is an interface element satisfying the condition (a), we note that $|\triangle A_4ED| \geqslant \sqrt{2}h|l|/4$ because the distance from A_4 to l is greater than $\sqrt{2}h/2$. Then we apply the standard trace inequality (3.4) to the term on the right hand side of (3.5) on the triangle $\triangle A_4ED$ to obtain

$$\begin{aligned} \|\sigma^-(\mathbf{c}_0 L)\| &\leqslant \frac{C|l|^{1/2}}{|l|^{1/2}\ |\triangle A_4ED|^{1/2}} \|\hat{\sigma}(\boldsymbol{\phi}_T^+)\|_{L^2(\triangle A_4ED)} \\ &\leqslant \frac{C}{|l|^{1/2}h^{1/2}} \left(\|(\mu^+ - \mu^-)\epsilon(\boldsymbol{\phi}_T^+)\|_{L^2(T^+)} + \|(\lambda^+ - \lambda^-)\nabla \cdot \boldsymbol{\phi}_T^+\|_{L^2(T^+)} \right) \\ &\leqslant \frac{C}{|l|^{1/2}h^{1/2}} \left(\frac{\mu_M}{\sqrt{\mu_m}} \|\sqrt{2\mu}\epsilon(\boldsymbol{\phi}_T)\|_{L^2(T)} + \frac{\lambda_M}{\sqrt{\lambda_m}} \|\sqrt{\lambda}\nabla \cdot \boldsymbol{\phi}_T\|_{L^2(T)} \right), \end{aligned} \tag{3.13}$$

which implies (3.12).

For an interface element T satisfying the condition (b) such that $|A_1E| \leqslant h/2$, i.e., $|A_3E| \geqslant h/2$. In such a case, we note that $|\triangle A_3ED| \geqslant \sqrt{2}h|l|/8$. Then, following similar arguments used for T satisfying the condition (a), we can obtain (3.12) by applying the standard trace inequality (3.4) to the term on the right hand side of (3.5) on the triangle $\triangle A_3ED$. Similar arguments apply when $|A_1D| \leqslant h/2$.

When T is an interface element satisfying condition (c), estimate (3.12) can be proved similarly. □

By Lemma 3.2, we can develop a stress trace inequality for IFE functions in the following theorem.

Theorem 3.1. *On every interface element T and its interface edge e whose normal is $\mathbf{n}_e$, the following inequality holds for every IFE function $\boldsymbol{\phi}_T(X)$:*

$$\|h^{1/2}\sigma(\boldsymbol{\phi}_T)\mathbf{n}_e\|_{L^2(e)} \leqslant C_t \left(\|\sqrt{2\mu}\epsilon(\boldsymbol{\phi}_T)\|_{L^2(T)} + \|\sqrt{\lambda}\nabla \cdot \boldsymbol{\phi}_T\|_{L^2(T)} \right), \tag{3.14}$$

where $C_t \leqslant \max\left\{\frac{\mu_M}{\sqrt{\mu_m}}, \frac{\lambda_M}{\sqrt{\lambda_m}}\right\}\widetilde{C}_t$ with $\widetilde{C}_t$ independent of the interface location and Lamé parameters.

Proof. We present our arguments for the rectangular and triangular elements separately.

Rectangular interface elements: Assuming that T is a Type 1 rectangular interface element illustrated in Figure 2.1, without loss of generality, we only consider the interface edge $e = A_1A_2 = A_1D \cup DA_2$ with

$A_1D \subset T^-$ and $DA_2 \subset T^+$. On the first piece A_1D of e, applying the trace inequality (3.4) on $\triangle A_1DA_3$ to the polynomial component $\boldsymbol{\phi}_T^-$, we have

$$\begin{aligned}\|h^{1/2}\sigma(\boldsymbol{\phi}_T)\mathbf{n}_e\|_{L^2(A_1D)} &= \|h^{1/2}\sigma^-(\boldsymbol{\phi}_T^-)\mathbf{n}_e\|_{L^2(A_1D)} \leqslant C\|\sigma^-(\boldsymbol{\phi}_T^-)\|_{L^2(\triangle A_1DA_3)}\\ &\leqslant C(\|\sigma^-(\boldsymbol{\phi}_T^-)\|_{L^2(\triangle A_1DE)} + \|\sigma^-(\boldsymbol{\phi}_T^-)\|_{L^2(\triangle A_3ED)})\\ &\leqslant C(\|\sigma^-(\boldsymbol{\phi}_T^-)\|_{L^2(T^-)} + \|\sigma^-(\boldsymbol{\phi}_T^+)\|_{L^2(\triangle A_3ED)} + \|\sigma^-(\mathbf{c}_0L)\|_{L^2(\triangle A_3ED)}),\end{aligned} \tag{3.15}$$

where we have used the relation (3.1) between $\boldsymbol{\phi}_T^-$ and $\boldsymbol{\phi}_T^+$ in the last inequality. The second term in the last inequality of (3.15) can be bounded by

$$\begin{aligned}\|\sigma^-(\boldsymbol{\phi}_T^+)\|_{L^2(\triangle A_3ED)} &\leqslant C\left(\|\mu^-\epsilon(\boldsymbol{\phi}_T^+)\|_{L^2(\triangle A_3ED)} + \|\lambda^-\nabla\cdot\boldsymbol{\phi}_T^+\|_{L^2(\triangle A_3ED)}\right)\\ &\leqslant C\left(\frac{\mu_M}{\sqrt{\mu_m}}\|\sqrt{2\mu^+}\epsilon(\boldsymbol{\phi}_T^+)\|_{L^2(T^+)} + \frac{\lambda_M}{\sqrt{\lambda_m}}\|\sqrt{\lambda^+}\nabla\cdot\boldsymbol{\phi}_T^+\|_{L^2(T^+)}\right).\end{aligned} \tag{3.16}$$

For the third term in the last inequality of (3.15), we note that $\sigma^-(\mathbf{c}_0L)$ is a constant tensor and $|\triangle A_3ED| \leqslant Ch|l|$. Then Lemma 3.2 implies

$$\begin{aligned}\|\sigma^-(\mathbf{c}_0L)\|_{L^2(\triangle A_3ED)} &= |\triangle A_3ED|^{1/2}\|\sigma^-(\mathbf{c}_0L)\|\\ &\leqslant C\left(\frac{\mu_M}{\sqrt{\mu_m}}\|\sqrt{2\mu}\epsilon(\boldsymbol{\phi}_T)\|_{L^2(T)} + \frac{\lambda_M}{\sqrt{\lambda_m}}\|\sqrt{\lambda}\nabla\cdot\boldsymbol{\phi}_T\|_{L^2(T)}\right).\end{aligned} \tag{3.17}$$

On the second piece DA_2 of e, applying the standard trace inequality (3.4) to the polynomial component $\boldsymbol{\phi}_T^+$ on $\triangle DA_2A_3$, we have

$$\begin{aligned}\|h^{1/2}\sigma(\boldsymbol{\phi}_T)\mathbf{n}_e\|_{L^2(DA_2)} &= \|h^{1/2}\sigma^+(\boldsymbol{\phi}_T^+)\mathbf{n}_e\|_{L^2(DA_2)} \leqslant C\|\sigma^+(\boldsymbol{\phi}_T^+)\|_{L^2(\triangle DA_2A_3)}\\ &\leqslant C\left(\frac{\mu_M}{\sqrt{\mu_m}}\|\sqrt{2\mu^+}\epsilon(\boldsymbol{\phi}_T^+)\|_{L^2(T^+)} + \frac{\lambda_M}{\sqrt{\lambda_m}}\|\sqrt{\lambda^+}\nabla\cdot\boldsymbol{\phi}_T^+\|_{L^2(T^+)}\right).\end{aligned} \tag{3.18}$$

Therefore (3.14) for the Type 1 rectangular interface element follows from (3.15)-(3.18) through the triangular inequality.

When T is a Type 2 rectangular interface element illustrated in Figure 2.1, we can simply apply the trace inequality (3.4) on $\triangle A_1DE$ and $\triangle DA_2E$:

$$\begin{aligned}\|h^{1/2}\sigma(\boldsymbol{\phi}_T)\mathbf{n}_e\|_{L^2(A_1D)} &= \|h^{1/2}\sigma^-(\boldsymbol{\phi}_T^-)\mathbf{n}_e\|_{L^2(A_1D)} \leqslant C\|\sigma^-(\boldsymbol{\phi}_T^-)\|_{L^2(\triangle A_1DE)}\\ &\leqslant C\left(\frac{\mu_M}{\sqrt{\mu_m}}\|\sqrt{2\mu^-}\epsilon(\boldsymbol{\phi}_T^-)\|_{L^2(T^-)} + \frac{\lambda_M}{\sqrt{\lambda_m}}\|\sqrt{\lambda^-}\nabla\cdot\boldsymbol{\phi}_T^-\|_{L^2(T^-)}\right),\end{aligned} \tag{3.19}$$

$$\begin{aligned}\|h^{1/2}\sigma(\boldsymbol{\phi}_T)\mathbf{n}_e\|_{L^2(DA_2)} &= \|h^{1/2}\sigma^+(\boldsymbol{\phi}_T^+)\mathbf{n}_e\|_{L^2(DA_2)} \leqslant C\|\sigma^+(\boldsymbol{\phi}_T^+)\|_{L^2(\triangle DA_2E)}\\ &\leqslant C\left(\frac{\mu_M}{\sqrt{\mu_m}}\|\sqrt{2\mu^+}\epsilon(\boldsymbol{\phi}_T^+)\|_{L^2(T^+)} + \frac{\lambda_M}{\sqrt{\lambda_m}}\|\sqrt{\lambda^+}\nabla\cdot\boldsymbol{\phi}_T^+\|_{L^2(T^+)}\right),\end{aligned} \tag{3.20}$$

which lead to (3.14) through the triangular inequality. In all the inequalities above, the generic constants C are independent of the interface location and Lamé parameters.

Triangular interface elements: Assuming T is a Type 1 triangular interface element illustrated in Figure 2.2, without loss of generality, we also only need to consider the interface edge A_1A_2. If $|A_1E| \leqslant h/2$, by Lemma 3.2, estimate (3.12) holds. Then (3.14) follows from arguments similar to those for (3.15)-(3.18). If $|A_1E| \geqslant h/2$, the proof reduces to the application of the standard trace inequality (3.4) on $\triangle A_1DE$ and $\triangle DA_2E$, and (3.14) follows from arguments similar to those for (3.19) and (3.20). The result for a Type 2 triangular interface element illustrated in Figure 2.2 can be proven similarly. □

Remark 3.1. *We highlight that the relation* (3.1) *together with the estimate* (3.12) *suggests the "closeness" of the two component polynomials in an IFE function, i.e., the difference of the two component polynomials of an IFE function is always bounded by an energy norm of the IFE function itself. On each interface element, although an IFE function is a piecewise polynomial, by this "closeness", its two component polynomials behave collectively like a standard polynomial, which, we believe, is the foundation that the stress trace inequality given in* (3.14) *can hold and is also the fundamental spirit in its proof.*

4 Approximation Capabilities In An Energy Norm

In this section, we consider the approximation capabilities of the elasticity IFE spaces, i.e., given a function $\mathbf{u}$, how well its interpolation $I_h\mathbf{u}$ in the IFE space can approximate $\mathbf{u}$. Recall from [21], the local IFE interpolation $I_{h,T} : \mathbf{PH}^2(T)/[H^2(T)]^2 \to \mathbf{S}_h(T),\ \forall T \in \mathcal{T}_h$ is defined in the following:

$$I_{h,T}\mathbf{u}(X) = \begin{cases} \sum_{i\in\mathcal{I}_T}[\boldsymbol{\psi}_{i,T}(X), \boldsymbol{\psi}_{i+|\mathcal{I}_T|,T}(X)]\mathbf{u}(A_i),\ \forall \mathbf{u} \in [H^2(T)]^2 & \text{if } T \in \mathcal{T}_h^n, \\ \sum_{i\in\mathcal{I}_T}[\boldsymbol{\phi}_{i,T}(X), \boldsymbol{\phi}_{i+|\mathcal{I}_T|,T}(X)]\mathbf{u}(A_i),\ \forall \mathbf{u} \in \mathbf{PH}^2(T) & \text{if } T \in \mathcal{T}_h^i, \end{cases} \tag{4.1}$$

where $\boldsymbol{\psi}_{i,T}, i \in \mathcal{I}_T$ are the standard Lagrange vector shape functions and $\boldsymbol{\phi}_{i,T}, i \in \mathcal{I}_T$ are the IFE shape functions given by (2.8). Similar interpolations are also used in discussions of IFE spaces for other interface problems, see, for examples, [18, 36, 53]. For every $\mathbf{u} \in \mathbf{PH}^2(\Omega)$, its global IFE interpolation $I_h\mathbf{u}$ over the domain Ω is defined piecewisely by $I_{h,T}\mathbf{u}, \forall T \in \mathcal{T}_h$ in the usual way. Our goal here is to extend the results in [21] to show the optimal approximation capabilities of the elasticity IFE spaces in the following energy norm:

$$\begin{aligned} |||\mathbf{v}|||_h^2 = &\sum_{T\in\mathcal{T}_h}\int_T 2\mu\|\epsilon(\mathbf{v})\|^2 dX + \sum_{T\in\mathcal{T}_h}\int_T \lambda\|\nabla\cdot\mathbf{v}\|^2 dX \\ &+ \sum_{e\in\mathcal{E}_h^i}\rho\int_e \|h^{-1/2}[\mathbf{v}]\|^2 ds + \sum_{e\in\mathcal{E}_h^i}\rho^{-1}\int_e \|h^{1/2}\{\sigma(\mathbf{v})\mathbf{n}_e\}\|^2 ds. \end{aligned} \tag{4.2}$$

To gauge the error of the IFE interpolation $I_h\mathbf{u}$ by the energy norm (4.2), we need to estimate the errors of the IFE interpolation $I_h\mathbf{u}$ on interface edges. Similar edge estimation is obtained in [38] for elliptic interface problems by assuming a $H^3(\Omega^{\pm})$ regularity for the function interpolated. Here, inspired by the ideas presented in [25, 26], we circumvent the excessive H^3 assumption by carrying out a related analysis on a patch or macro-element around each interface element so that an error bound in the optimal order can be derived under the usual H^2 regularity assumption for $\mathbf{u}$. We also note that the interpolation operator in [26] is based on projection and a discontinuous Galerkin formulation is used around the interface, but here we use the Lagrange type interpolation because the IFE functions are continuous at mesh nodes.

4.1 Multipoint Taylor Expansions

In this subsection, we establish a group of multipoint Taylor expansions for vector functions satisfying the jump conditions (1.1b) and (1.1c) on the patch of each interface element which will be used to investigate the approximation capability of the IFE spaces by deriving error estimates for the related Lagrange interpolation. Specifically, for each interface element $T \in \mathcal{T}_h^i$, its patch or macro-element is the following set:

$$\omega_T = \bigcup\Big\{T' \in \mathcal{T}_h : T' \cap T \neq \emptyset\Big\}. \tag{4.3}$$

In addition, we assume the patch of each interface element has the following property:

Patch Assumption: For every interface element T, let e be one of the interface edge of T. Then for $s = \pm$, there exists a triangle $T_e^s \subset \Omega^s \cap \omega_T$ and two constants C_1, C_2 independent of the interface location such that $e \cap T^s$ is one edge of T_e^s and

$$C_1|e \cap T^s|h \leqslant |T_e^s| \leqslant C_2|e \cap T^s|h. \tag{4.4}$$

In fact, (4.4) can be guaranteed if the height of the auxiliary triangle T_e^s corresponding to the edge $e \cap T^s$ has the length $\mathcal{O}(h)$, and we note that this Patch Assumption can be easily satisfied when the mesh size h is sufficient small such that the interface is locally flat enough. Figure 4.1 provides illustrations for how $T_e^s, s = \pm$ are identified for an interface edge $e = A_1A_2$ in the patch ω_T of an interface element $T = \triangle A_1A_2A_3$ with $A_1 \in \Omega^-$ and $A_2 \in \Omega^+$, where $T_e^- = \triangle A_1PD$, $T_e^+ = \triangle A_2QD$ when T is of Type 1, and $T_e^- = \triangle A_1DA_3$, $T_e^+ = A_2DP$ when T is of Type 2, respectively. The auxiliary triangles $T_e^s, s = \pm$ do not have to be formed by nodes in the mesh $\mathcal{T}_h$. For example, the point P in Type 1 in Figure 4.1 can be a point in $\overline{\omega}_T \cap \Omega^-$ so long as its perpendicular distance to the line passing e is $\mathcal{O}(h)$.

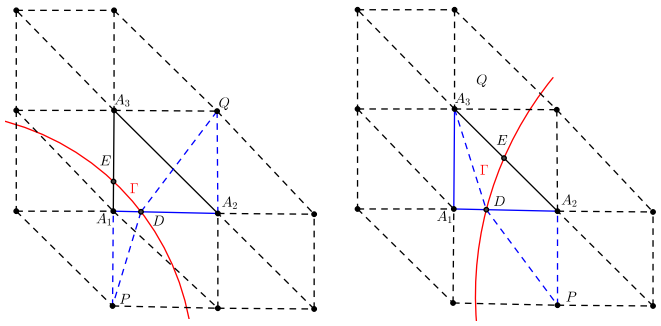

(a) Type 1 (b) Type 2

Figure 4.1: The patch for a triangular interface element $T = \triangle A_1A_2A_3$

The multi-point Taylor expansion presented in the following is essentially the same as the one used in [21] except that the arguments are used on the patch whose area is larger than the interface element itself. In the discussions from now on, for any two tensors $A = (a_{ij})_{i,j=1}^{m,n}$ and $B = (b_{ij})_{i,j=1}^{m,n}$, we let $A : B = \sum_{i,j=1}^{m,n} a_{ij}\ b_{ij}$, and we will adopt the following Kronecker product and vectorization operations:

$$A \otimes B = \begin{bmatrix} a_{11}B & \cdots & a_{1n}B \\ \vdots & \ddots & \vdots \\ a_{m1}B & \cdots & a_{mn}B \end{bmatrix}, \quad \mathrm{Vec}(A) = [a_{11}, \cdots, a_{m1}, \cdots, a_{1n}, \cdots, a_{mn}]^T. \tag{4.5}$$

For each interface element described by vertices A_i, $i \in \mathcal{I}_T$, without loss of generality, we partition the index set $\mathcal{I}_T$ into two sub-index sets $\mathcal{I}_T^+ = \{i : A_i \in T^+\}$ and $\mathcal{I}_T^- = \{i : A_i \in T^-\}$. Let l be the line determined by two intersection points D and E of Γ and ∂T with the normal vector $\bar{\mathbf{n}} = (\bar{n}_1, \bar{n}_2)$. The interface Γ and the line l partition the patch ω_T into sub-patches $\omega_T^s, s = \pm$ and $\hat{\omega}_T^s, s = \pm$, respectively. Let $\widetilde{\omega}_T^s = \omega_T^s \cap \hat{\omega}_T^s$, $s = \pm$. Then $\widetilde{\omega}_T = (\widetilde{\omega}_T^+ \cap \omega_T^-) \cup (\widetilde{\omega}_T^- \cap \omega_T^+)$ is the sub-patch sandwiched between l and Γ. In addition, following the idea in [21, 24], we consider the following set

$$\omega_T^{int} = \bigcup \{l_t \cap \omega_T : l_t \text{ is a tangent line to } \omega_T \cap \Gamma\}. \tag{4.6}$$

For every vertex A_i of T and each point $X \in \omega_T \backslash \omega_T^{int}$, the line segment A_iX intersects $\Gamma \cap \omega_T$ either with no point or only one point. In the first case, A_i and X must be on the same side of $\Gamma \cap T$, while in

the second case, they are on different sides. In order to describe the Taylor expansions, we further define $\omega_T^{*,s} = \tilde{\omega}_T^s \backslash \omega_T^{int}$, $s = \pm$, and $\omega_T^* = \omega_T \backslash (\omega_T^{*,-} \cup \omega_T^{*,+})$.

Following Lemma 3.4 in [21], we can show that $|\omega_T^*| \leqslant Ch^3$ provided that the mesh size is small enough. This geometric feature allows us to employ a second order expansion on $\omega_T^{*,s}$, $s = \pm$, but a first order expansion on ω_T^* because $|\omega_T^*| \leqslant Ch^3$ can compensate the lower order accuracy of the first order expansion.

For every $X \in \omega_T^{*,s}$, let $Y_i(t, X) = tA_i + (1-t)X$, $t \in [0,1]$, $i \in \mathcal{I}$, and let $\tilde{t}_i = \tilde{t}_i(X) \in [0,1]$ be such that $\widetilde{Y}_i = Y_i(\tilde{t}_i, X)$ is on the curve $\Gamma \cap T$ if X and A_i are on different sides of T. Besides, we let $\mathbf{n}(\widetilde{X})$ be the normal vector to Γ at every $\widetilde{X} \in \Gamma \cap \omega_T$, and denote $\widetilde{X}^\perp$ as the projection of $\widetilde{X}$ onto l. Following Lemma 3.1 and Lemma 3.2 in [18], given any $\widetilde{X} \in \Gamma \cap \omega_T$, we can show the following geometric estimate:

$$\|\widetilde{X} - \widetilde{X}^\perp\| \leqslant Ch^2, \quad \|\mathbf{n}(\widetilde{X}) - \bar{\mathbf{n}}\| \leqslant Ch. \tag{4.7}$$

In the discussions from now on, s and s' take opposite signs, i.e., whenever $s = \pm$, then $s' = \mp$, and vice versa. Following the same procedure used for the results in Theorem 5.5 in [21], we can establish the following multi-point Taylor expansions for $I_{h,T}\mathbf{u} - \mathbf{u}$:

$$\partial_{x_d}(I_{h,T}\mathbf{u}(X) - \mathbf{u}(X)) = \sum_{i \in \mathcal{I}^{s'}} \big(\partial_{x_d}\Phi_{i,T}(X)\big)(\mathbf{E}_i^s + \mathbf{F}_i^s) + \sum_{i \in \mathcal{I}} \big(\partial_{x_d}\Phi_{i,T}(X)\big)\mathbf{R}_i^s, \ \forall X \in \omega_T^{*,s}, \ s = \pm, \tag{4.8}$$

$$\partial_{x_d x_{d'}} I_{h,T}\mathbf{u}(X) = \sum_{i \in \mathcal{I}^{s'}} \big(\partial_{x_d x_{d'}}\Phi_{i,T}(X)\big)(\mathbf{E}_i^s + \mathbf{F}_i^s) + \sum_{i \in \mathcal{I}} \big(\partial_{x_d x_{d'}}\Phi_{i,T}(X)\big)\mathbf{R}_i^s, \ \forall X \in \omega_T^{*,s}, \ s = \pm, \tag{4.9}$$

$$\partial_{x_d} I_{h,T}\mathbf{u}(X) = \sum_{i \in \mathcal{I}} \big(\partial_{x_d}\Phi_{i,T}(X)\big)\widetilde{\mathbf{R}}_i, \ \forall X \in \omega_T^*, \tag{4.10}$$

$$\partial_{x_d x_{d'}} I_{h,T}\mathbf{u}(X) = \sum_{i \in \mathcal{I}} \big(\partial_{x_d x_{d'}}\Phi_{i,T}(X)\big)\widetilde{\mathbf{R}}_i, \ \forall X \in \omega_T^*, \tag{4.11}$$

where $d, d' = 1, 2$, $\Phi_{i,T} = [\boldsymbol{\phi}_{i,T}, \boldsymbol{\phi}_{i+|\mathcal{I}_T|,T}]$ and

$$\mathbf{R}_i^s(X) = \int_0^1 (1-t)\frac{d^2}{dt^2}\mathbf{u}^s(Y_i(t,X))dt, \ i \in \mathcal{I}^s, \tag{4.12}$$

$$\mathbf{R}_i^s(X) = \mathbf{R}_{i1}^s(X) + \mathbf{R}_{i2}^s(X) + \mathbf{R}_{i3}^s(X), \ i \in \mathcal{I}^{s'}, \quad \begin{cases} \mathbf{R}_{i1}^s(X) = \int_0^{\tilde{t}_i}(1-t)\frac{d^2}{dt^2}\mathbf{u}^s(Y_i(t,X))dt, \\ \mathbf{R}_{i2}^s(X) = \int_{\tilde{t}_i}^1(1-t)\frac{d^2}{dt^2}\mathbf{u}^{s'}(Y_i(t,X))dt, \\ \mathbf{R}_{i3}^s(X) = (1-\tilde{t}_i)((A_i - X)^T \otimes I_2)\cdot \\ \quad (M^s(\widetilde{Y}_i) - I_4)\int_0^{\tilde{t}_i}\frac{d}{dt}\,Vec\left(\nabla\mathbf{u}^s(Y_i(t,X))\right)dt, \end{cases} \tag{4.13}$$

$$\mathbf{E}_i^s(X) = \left((A_i - \widetilde{Y}_i)^T \otimes I_2\right)\left(M^s(\widetilde{Y}_i) - \overline{M}^s\right)\mathrm{Vec}(\nabla\mathbf{u}^s(X)), \tag{4.14}$$

$$\mathbf{F}_i^s(X) = -\left((\widetilde{Y}_i - \widetilde{Y}_i^\perp)^T \otimes I_2\right)\left(\overline{M}^s - I_4\right)\mathrm{Vec}(\nabla\mathbf{u}^s(X)), \tag{4.15}$$

$$\widetilde{\mathbf{R}}_i(X) = \int_0^1 \frac{d}{dt}\mathbf{u}(Y_i(t,X))dt \tag{4.16}$$

and $\overline{M}^- = \left(\overline{N}^+\right)^{-1}\overline{N}^-$, $\overline{M}^+ = \left(\overline{N}^-\right)^{-1}\overline{N}^+$, with

$$N^s(\widetilde{X}) = \begin{bmatrix} (\lambda^s + 2\mu^s)\tilde{n}_1(\widetilde{X}) & \mu^s\tilde{n}_2(\widetilde{X}) & \mu^s\tilde{n}_2(\widetilde{X}) & \lambda^s\tilde{n}_1(\widetilde{X}) \\ \lambda^s\tilde{n}_2(\widetilde{X}) & \mu^s\tilde{n}_1(\widetilde{X}) & \mu^s\tilde{n}_1(\widetilde{X}) & (\lambda^s + 2\mu^s)\tilde{n}_2(\widetilde{X}) \\ -\tilde{n}_2(\widetilde{X}) & 0 & \tilde{n}_1(\widetilde{X}) & 0 \\ 0 & -\tilde{n}_2(\widetilde{X}) & 0 & \tilde{n}_1(\widetilde{X}) \end{bmatrix}, \quad s = \pm, \tag{4.17}$$

$$\overline{N}^s = \begin{bmatrix} (\lambda^s+2\mu^s)\bar{n}_1 & \mu^s\bar{n}_2 & \mu^s\bar{n}_2 & \lambda^s\bar{n}_1 \\ \lambda^s\bar{n}_2 & \mu^s\bar{n}_1 & \mu^s\bar{n}_1 & (\lambda^s+2\mu^s)\bar{n}_2 \\ -\bar{n}_2 & 0 & \bar{n}_1 & 0 \\ 0 & -\bar{n}_2 & 0 & \bar{n}_1 \end{bmatrix}, \quad s=\pm. \tag{4.18}$$

4.2 Estimates For The Interpolation Error

In this subsection, using the expansions in the previous subsection, we derive various estimates for errors of the IFE interpolation, especially the one in the energy norm. First of all, we prove the following estimate for the IFE interpolation on ω_T.

Theorem 4.1. *Assume the mesh $\mathcal{T}_h$ is sufficiently fine, then there exists a constant C independent of the interface location such that the following estimate holds on the patch ω_T of every interface element T:*

$$\|\nabla(I_{h,T}\mathbf{u}-\mathbf{u})\|_{L^2(\omega_T)} + h\|\nabla^2(I_{h,T}\mathbf{u}-\mathbf{u})\|_{L^2(\omega_T)} \leqslant Ch(\|\mathbf{u}\|_{\mathbf{PH}^2(\omega_T)} + \|\mathbf{u}\|_{\mathbf{PW}^{1,6}(\omega_T)}) \tag{4.19}$$

provided that $\mathbf{u} \in \mathbf{PH}^2(\omega_T)$.

Proof. The proof essentially follows from the same arguments as those for Theorem 5.7 and Theorem 5.8 in [21]. Consider the estimation on $\omega_T^{*,s}$ first. According to $\|X - A_i\| \leqslant Ch$, $i \in \mathcal{I}$ for any $X \in \omega_T$, we can use Lemmas 4.1 and 4.2 in [21] to show that

$$\|\mathbf{R}_i^s\|_{L^2(\omega_T^{*,s})} \leqslant Ch^2\|\mathbf{u}\|_{\mathbf{PH}^2(\omega_T)}, \quad s=\pm,\ \forall i \in \mathcal{I}. \tag{4.20}$$

Because of (4.7), we have $\|M^s(\widetilde{Y}_i) - \overline{M}^s\| \leqslant Ch$, $i \in \mathcal{I}$, $s=\pm$, and thus

$$\|\mathbf{E}_i^s\|_{L^2(\omega_T^{*,s})} \leqslant C\|(A_i - \widetilde{Y}_i)\|\|M^s(\widetilde{Y}_i) - \overline{M}^s\|\|\nabla\mathbf{u}^s\|_{L^2(\omega_T^{*,s})} \leqslant Ch^2\|\mathbf{u}\|_{\mathbf{PH}^2(\omega_T)}. \tag{4.21}$$

Using (4.7) again, for $i \in \mathcal{I}$, $s=\pm$, we have

$$\|\mathbf{F}_i^s\|_{L^2(\omega_T^{*,s})} \leqslant C\|\widetilde{Y}_i - \widetilde{Y}_i^{\perp}\|\|\overline{M}^s - I_4\|\|\nabla\mathbf{u}^s\|_{L^2(\omega_T^{*,s})} \leqslant Ch^2\|\mathbf{u}\|_{\mathbf{PH}^2(\omega_T)}. \tag{4.22}$$

By applying the estimates given in (4.20)-(4.22) with the bounds for the IFE shape functions, i.e., $|\boldsymbol{\phi}_{i,T}|_{W^{k,\infty}(\omega_T)} \leqslant Ch^{-k}$, $k=1,2$ given by Theorem 5.2 in [21] to the multi-point Taylor expansions (4.8) and (4.9), we have

$$\begin{aligned} \|\partial_{x_d}(I_{h,T}\mathbf{u}-\mathbf{u})\|_{L^2(\omega_T^{*,s})} &\leqslant Ch^{-1}\left(\sum_{i\in\mathcal{I}^{s'}}(\|\mathbf{E}_i^s\|_{L^2(\omega_T^{*,s})} + \|\mathbf{F}_i^s\|_{L^2(\omega_T^{*,s})}) + \sum_{i\in\mathcal{I}}\|\mathbf{R}_i^s\|_{L^2(\omega_T^{*,s})}\right) \\ &\leqslant Ch\|\mathbf{u}\|_{\mathbf{PH}^2(\omega_T)},\ d=1,2,\ s=\pm, \end{aligned} \tag{4.23}$$

$$\begin{aligned} \|\partial_{x_dx_{d'}}(I_{h,T}\mathbf{u}-\mathbf{u})\|_{L^2(\omega_T^{*,s})} &\leqslant Ch^{-2}\left(\sum_{i\in\mathcal{I}^{s'}}(\|\mathbf{E}_i^s\|_{L^2(\omega_T^{*,s})} + \|\mathbf{F}_i^s\|_{L^2(\omega_T^{*,s})}) + \sum_{i\in\mathcal{I}}\|\mathbf{R}_i^s\|_{L^2(\omega_T^{*,s})}\right) \\ &\quad + \|\partial_{x_dx_{d'}}\mathbf{u}\|_{L^2(\omega_T^{*,s})} \leqslant C\|\mathbf{u}\|_{\mathbf{PH}^2(\omega_T)},\ d,d'=1,2,\ s=\pm. \end{aligned} \tag{4.24}$$

For the estimation on ω_T^*, following the same arguments used for Lemma 4.3 and Theorem 5.8 in [21] and using the estimate $|\omega_T^*| \leqslant Ch^3$, $\|X - A_i\| \leqslant Ch$, $\forall X \in \omega_T$, we can prove

$$\begin{aligned} &\|\widetilde{\mathbf{R}}_i\|_{L^2(\omega_T^*)} \leqslant Ch^2\|\mathbf{u}\|_{\mathbf{PW}^{1,6}(\omega_T)}, \\ \text{and}\quad &\|\partial_{x_d}\mathbf{u}\|_{L^2(\omega_T^*)} \leqslant Ch\|\mathbf{u}\|_{\mathbf{PW}^{1,6}(\omega_T)}, \quad \|\partial_{x_dx_{d'}}\mathbf{u}\|_{L^2(\omega_T^*)} \leqslant C\|\mathbf{u}\|_{\mathbf{PW}^{1,6}(\omega_T)}, \end{aligned} \tag{4.25}$$

where we have used the fact that $H^2(\omega_T^s) \subseteq W^{1,6}(\omega_T^s)$, $s = \pm$. Then, by the multi-point Taylor expansions (4.10) and (4.11) and using the bounds for the IFE shape functions again, we obtain

$$\|\partial_{x_d}(I_{h,T}\mathbf{u} - \mathbf{u})\|_{L^2(\omega_T^*)} \leqslant Ch^{-1}\left(\sum_{i\in\mathcal{I}} \|\widetilde{\mathbf{R}}_i\|_{L^2(\omega_T^*)}\right) + \|\partial_{x_d}\mathbf{u}\|_{L^2(\omega_T^*)} \leqslant Ch\|\mathbf{u}\|_{\mathbf{PW}^{1,6}(\omega_T)}, \tag{4.26}$$

$$\begin{aligned}\|\partial_{x_d x_{d'}}(I_{h,T}\mathbf{u} - \mathbf{u})\|_{L^2(\omega_T^*)} &\leqslant Ch^{-2}\left(\sum_{i\in\mathcal{I}} \|\widetilde{\mathbf{R}}_i\|_{L^2(\omega_T^*)}\right) + \|\partial_{x_d x_{d'}}\mathbf{u}\|_{L^2(\omega_T^*)} \\ &\leqslant C(\|\mathbf{u}\|_{\mathbf{PW}^{1,6}(\omega_T)} + \|\mathbf{u}\|_{\mathbf{PH}^2(\omega_T)}), \quad d, d' = 1, 2.\end{aligned} \tag{4.27}$$

Finally, (4.19) follows from (4.23), (4.24), (4.26) and (4.27). □

Using the Patch Assumption and the estimate (4.19), we can estimate the interpolation errors on interface edges as follows.

Theorem 4.2. *Assume the mesh $\mathcal{T}_h$ is sufficiently fine and satisfies the Patch Assumption. Then, there exists a constant C independent of the relative interface location such that the following estimate holds:*

$$\sum_{e\in\mathring{\mathcal{E}}_h^i} \|\{\sigma(\mathbf{u} - I_h\mathbf{u})\}\mathbf{n}_e\|_{L^2(e)} \leqslant Ch^{1/2}\|\mathbf{u}\|_{\mathbf{PH}^2(\Omega)}, \quad \forall \mathbf{u} \in \mathbf{PH}^2(\Omega). \tag{4.28}$$

Proof. For each $T \in \mathcal{T}_h^i$, let $e \in \mathring{\mathcal{E}}_h^i$ be one interface edge of T and let $e^s = e \cap \Omega^s$, $s = \pm$. According to the Patch Assumption, there exist triangles T_e^s inside the patch ω_T of T with e^s as one of its edge such that $T_e^s \subset \Omega^s$ and $C_1 h \leqslant |T_e^s|/|e^s|$. Then, we apply the standard trace inequality on T_e^s and use the estimate in (4.19) to obtain

$$\begin{aligned}\|\nabla(I_{h,T}\mathbf{u} - \mathbf{u})\|_{L^2(e^s)} &\leqslant C|e^s|^{1/2}/|T_e^s|^{1/2}\left(\|\nabla(I_{h,T}\mathbf{u} - \mathbf{u})\|_{L^2(T_e^s)} + h\|\nabla^2(I_{h,T}\mathbf{u} - \mathbf{u})\|_{L^2(T_e^s)}\right) \\ &\leqslant Ch^{1/2}(\|\mathbf{u}\|_{\mathbf{PH}^2(\omega_T)} + \|\mathbf{u}\|_{\mathbf{PW}^{1,6}(\omega_T)}).\end{aligned} \tag{4.29}$$

For each $e \in \mathring{\mathcal{E}}_h^i$, let T_e^1 and T_e^2 be the two interface elements sharing e, then (4.29) implies

$$\begin{aligned}\sum_{e\in\mathring{\mathcal{E}}_h^i} \|\{\sigma(\mathbf{u} - I_h\mathbf{u})\}\mathbf{n}_e\|_{L^2(e)} &\leqslant C\sum_{e\in\mathring{\mathcal{E}}_h^i}\left(\|\nabla(I_{h,T_e^1}\mathbf{u} - \mathbf{u})\|_{L^2(e)} + \|\nabla(I_{h,T_e^1}\mathbf{u} - \mathbf{u})\|_{L^2(e)}\right) \\ &\leqslant Ch^{1/2}\sum_{e\in\mathring{\mathcal{E}}_h^i}\sum_{j=1,2}\left(\|\mathbf{u}\|_{\mathbf{PH}^2(\omega_{T_e^j})} + \|\mathbf{u}\|_{\mathbf{PW}^{1,6}(\omega_{T_e^j})}\right) \\ &\leqslant Ch^{1/2}(\|\mathbf{u}\|_{\mathbf{PH}^2(\Omega)} + \|\mathbf{u}\|_{\mathbf{PW}^{1,6}(\Omega)}),\end{aligned} \tag{4.30}$$

where we have used the finite overlapping property of ω_T, $T \in \mathcal{T}_h^i$. Finally, we obtain (4.28) by applying the standard imbedding inequality $\|w\|_{W^{1,6}(\Omega^s)} \leqslant C\|w\|_{H^2(\Omega^s)}$ [43], $\forall w \in W^{1,6}(\Omega^s)$, $s = \pm$ to (4.30) with $w = u_1$ and u_2. □

Now we are ready to gauge the error in the IFE interpolation by the energy norm $|||\cdot|||_h$.

Theorem 4.3. *Assume the mesh $\mathcal{T}_h$ is sufficiently fine and satisfies the Patch Assumption. Then there exists a constant C independent of the interface location such that the following estimate holds:*

$$|||I_h\mathbf{u} - \mathbf{u}|||_h \leqslant Ch\|\mathbf{u}\|_{\mathbf{PH}^2(\Omega)}, \ \forall \mathbf{u} \in \mathbf{PH}^2(\Omega). \tag{4.31}$$

Proof. According to the interpolation error estimation in terms of H^1 norm given by Theorem 5.9 in [21], we directly have

$$\sum_{T\in\mathcal{T}_h}\int_T 2\mu\|\epsilon(I_h\mathbf{u}-\mathbf{u})\|^2dX+\sum_{T\in\mathcal{T}_h}\int_T\lambda\|\nabla\cdot(I_h\mathbf{u}-\mathbf{u})\|^2dX\leqslant Ch^2\|\mathbf{u}\|^2_{\mathbf{PH}^2(\Omega)}. \tag{4.32}$$

In addition, since $I_h\mathbf{u}-\mathbf{u}\in\left[H^1(T)\right]^2$ for each interface element $T\in\mathcal{T}_h^i$, we apply the trace inequality and the approximation capability of Theorem 5.9 in [21] to obtain

$$\begin{aligned}\sum_{e\in\mathring{\mathcal{E}}_h^i}\int_e\|h^{-1/2}[I_h\mathbf{u}-\mathbf{u}]\|^2ds&\leqslant Ch^{-1}\sum_{e\in\mathring{\mathcal{E}}_h^i}\sum_{j=1,2}\|(I_h\mathbf{u}-\mathbf{u})|_{T_e^j}\|^2_{L^2(e)}\\&\leqslant Ch^{-2}\sum_{e\in\mathring{\mathcal{E}}_h^i}\sum_{j=1,2}\left(\|I_h\mathbf{u}-\mathbf{u}\|^2_{L^2(T_e^j)}+h^2\|\nabla(I_h\mathbf{u}-\mathbf{u})\|^2_{L^2(T_e^j)}\right)\\&\leqslant Ch^{-2}\left(\|I_h\mathbf{u}-\mathbf{u}\|^2_{L^2(\Omega)}+h^2\|\nabla(I_h\mathbf{u}-\mathbf{u})\|^2_{L^2(\Omega)}\right)\\&\leqslant Ch^2\|\mathbf{u}\|^2_{\mathbf{PH^2}(\Omega)},\end{aligned} \tag{4.33}$$

where T_e^1 and T_e^2 are the two elements sharing the interface edge e. Finally, estimate (4.31) follows from applying (4.33), (4.32) and Theorem 4.2 to $|||I_h\mathbf{u}-\mathbf{u}|||_h$ according to the definition of $|||\cdot|||_h$ given in (4.2).□

5 Errors Estimation For The PPIFE Method

In this section, we show that the IFE solution generated by the PPIFE scheme (2.17) can converge to the exact solution of the interface problem (1.1a)-(1.1e) with optimal convergence rates in terms of the polynomial space involved in the corresponding IFE spaces. First of all, we show that $|||\cdot|||_h$ in (4.2) is a norm of the space $\mathbf{V}_h$.

Lemma 5.1. *$|||\cdot|||_h$ is a norm of $\mathbf{V}_h$.*

Proof. It is obvious that $|||\cdot|||_h$ is a semi-norm of the space $\mathbf{V}_h$; hence, we only need to show that $|||\mathbf{v}|||_h\neq 0$ for every nonzero $\mathbf{v}\in\mathbf{V}_h$. Suppose $|||\mathbf{v}|||_h=0$ for some $\mathbf{v}\in\mathbf{V}_h(\Omega)$, then $\|\epsilon(\mathbf{v})\|_{L^2(T)}=0$ for every $T\in\mathcal{T}_h$. Thus, by direct application of calculus, $\mathbf{v}=\mathbf{p}_T+q_T(-x_2,x_1)^T$ on each non-interface element $T\in\mathcal{T}_h^n$, and $\mathbf{v}=\mathbf{p}_T^s+q_T^s(-x_2,x_1)^T$ on T^s, $s=\pm$ on each interface element $T\in\mathcal{T}_h^i$, where q_T, q_T^s and $\mathbf{p}_T=(p_T^1,p_T^2)^T$, $\mathbf{p}_T^s=(p_T^{s,1},p_T^{s,2})^T$ are some constants (vectors). The continuity on interior non-interface edges and $\|h^{-1/2}[\mathbf{v}]\|=0$ on every $e\in\mathring{\mathcal{E}}_h^i$ yield that $\mathbf{p}_T=\mathbf{p}_T^s=\mathbf{p}$ and $q_T=q_T^s=q$ for all the elements $T\in\mathcal{T}_h$ for some constant q and vector $\mathbf{p}$. Since $\mathbf{v}|_{\partial\Omega_D}=\mathbf{0}$, we have $\mathbf{p}=\mathbf{0}$, $q=0$ and thus $\mathbf{v}=\mathbf{0}$ on Ω.□

Then, we show the coercivity and continuity for the bilinear form $a_h(\cdot,\cdot)$ defined by (2.15) in terms of the norm $|||\cdot|||_h$.

Theorem 5.1. *For $\theta=-1$, 1 or 0, the following inequality holds for ρ sufficiently large:*

$$a_h(\mathbf{v},\mathbf{v})\geqslant\frac{1}{2}|||\mathbf{v}|||_h^2,\quad\forall\mathbf{v}\in\mathbf{S}_h(\Omega), \tag{5.1}$$

which implies that the bilinear form $a_h(\cdot,\cdot)$ is coercive on $\mathbf{S}_h(\Omega)$.

Proof. Letting $\mathbf{u} = \mathbf{v}$ in (2.15), we have

$$\begin{aligned} a_h(\mathbf{v},\mathbf{v}) = &\sum_{T\in\mathcal{T}_h}\int_T \|\sqrt{2\mu}\epsilon(\mathbf{v})\|^2 dX + \sum_{T\in\mathcal{T}_h}\int_T \|\sqrt{\lambda}\nabla\cdot\mathbf{v}\|^2 dX \\ &+ (\theta-1)\sum_{e\in\mathring{\mathcal{E}}_h^i}\int_e \{\sigma(\mathbf{v})\mathbf{n}_e\}\cdot[\mathbf{v}]ds + \sum_{e\in\mathring{\mathcal{E}}_h^i}\rho\int_e \|h^{-1/2}[\mathbf{v}]\|^2 ds. \end{aligned} \tag{5.2}$$

We only need to bound the third term in (5.2). For each interface edge $e \in \mathring{\mathcal{E}}_h^i$, let T_e^1 and T_e^2 be the interface elements sharing e. Firstly, we note that the stress trace inequality in Theorem 3.1 yields

$$\|h^{1/2}\{\sigma(\mathbf{v})\mathbf{n}_e\}\|_{L^2(e)}^2 \leqslant \frac{C_t^2}{2}\sum_{i=1,2}\left(\|\sqrt{2\mu}\epsilon(\mathbf{v})\|_{L^2(T_e^i)}^2 + \|\sqrt{\lambda}\nabla\cdot\mathbf{v}\|_{L^2(T_e^i)}^2\right). \tag{5.3}$$

Then, by (5.3), Hölder's inequality, and Young's inequality, we have

$$\begin{aligned} \int_e \{\sigma(\mathbf{v})\mathbf{n}_e\}\cdot[\mathbf{v}]ds &\leqslant \|\{\sigma(\mathbf{v})\mathbf{n}_e\}\|_{L^2(e)}\|h^{-1/2}[\mathbf{v}_h]\|_{L^2(e)} \\ &\leqslant \frac{C_t}{2}\left(\sum_{i=1,2}\|\sqrt{2\mu}\epsilon(\mathbf{v})\|_{L^2(T_e^i)} + \|\sqrt{\lambda}\nabla\cdot\mathbf{v}\|_{L^2(T_e^i)}\right)\|h^{-1/2}[\mathbf{v}_h]\|_{L^2(e)} \\ &\leqslant \frac{\alpha}{2}\left(\sum_{i=1,2}\|\sqrt{2\mu}\epsilon(\mathbf{v})\|_{L^2(T_e^i)}^2 + \|\sqrt{\lambda}\nabla\cdot\mathbf{v}\|_{L^2(T_e^i)}^2\right) + \frac{C_t^2}{2\alpha}\|h^{-1/2}[\mathbf{v}_h]\|_{L^2(e)}^2, \end{aligned} \tag{5.4}$$

where $\alpha > 0$ and the constant C_t is from the the trace inequality in Theorem 3.1. Since $|\theta - 1| \leq 2$, substituting (5.4) into (5.2) leads to

$$\begin{aligned} a_h(\mathbf{v},\mathbf{v}) \geqslant (1-\alpha)&\left(\sum_{T\in\mathcal{T}}\|\sqrt{2\mu}\epsilon(\mathbf{v})\|_{L^2(T)}^2 + \sum_{T\in\mathcal{T}_h}\|\sqrt{\lambda}\nabla\cdot\mathbf{v}\|_{L^2(T)}^2\right) \\ &+ \sum_{e\in\mathring{\mathcal{E}}_h^i}\left(\rho - \frac{C_t^2}{\alpha}\right)\|h^{-1/2}[\mathbf{v}]\|_{L^2(e)}^2. \end{aligned} \tag{5.5}$$

Then, by adding and subtracting $\sum_{e\in\mathring{\mathcal{E}}_h^i}\rho^{-1}\|\{\sigma(\mathbf{v})\mathbf{n}_e\}\|_{L^2(e)}^2$ in (5.5), and applying (5.3), we have

$$\begin{aligned} a_h(\mathbf{v},\mathbf{v}) \geqslant \left(1-\alpha-\frac{C_t^2}{\rho}\right)&\left(\sum_{T\in\mathcal{T}}\|\sqrt{2\mu}\epsilon(\mathbf{v})\|_{L^2(T)}^2 + \sum_{T\in\mathcal{T}_h}\|\sqrt{\lambda}\nabla\cdot\mathbf{v}_h\|_{L^2(T)}^2\right) \\ &+ \sum_{e\in\mathring{\mathcal{E}}_h^i}\rho^{-1}\|h^{1/2}\{\sigma(\mathbf{v})\mathbf{n}_e\}\|_{L^2(e)}^2 + \sum_{e\in\mathring{\mathcal{E}}_h^i}\left(\rho-\frac{C_t^2}{\alpha}\right)\|h^{-1/2}[\mathbf{v}]\|_{L^2(e)}^2. \end{aligned} \tag{5.6}$$

Finally, by letting $\alpha = 1/4$ and $\rho \geq 4C_t^2 + 1/2$ in (5.6), we have the coercivity (5.1). □

Remark 5.1. *According to Theorem 3.1 and the proof above, for $a_h(\cdot,\cdot)$ in the SPPIFE, NPPIFE, and IPPIFE methods to be coercive, it is sufficient to choose ρ such that*

$$\rho \geqslant 4\max\left\{\frac{\mu_M^2}{\mu_m}, \frac{\lambda_M^2}{\lambda_m}\right\}\widetilde{C}_t^2 + \frac{1}{2}, \tag{5.7}$$

where $\widetilde{C}_t$ is independent of the interface location and Lamé parameters.

Theorem 5.2. *There exists a constant $\beta \leq 5$ such that for every $\mathbf{w}, \mathbf{v} \in \mathbf{V}_h$, there holds*

$$a_h(\mathbf{w}, \mathbf{v}) \leqslant \beta |||\mathbf{w}|||_h |||\mathbf{v}|||_h, \forall\ \mathbf{w}, \mathbf{v} \in \mathbf{V}_h, \tag{5.8}$$

and this implies that the bilinear form $a_h(\cdot, \cdot)$ is continuous on $\mathbf{V}_h$.

Proof. According to the definition (2.15), we have

$$\begin{aligned} a_h(\mathbf{w}, \mathbf{v}) = &\sum_{T \in \mathcal{T}_h} \int_T 2\mu \epsilon(\mathbf{w}) : \epsilon(\mathbf{v}) dX + \sum_{T \in \mathcal{T}_h} \int_T \lambda (\nabla \cdot \mathbf{w})(\nabla \cdot \mathbf{v}) dX \\ &+ \theta \sum_{e \in \mathring{\mathcal{E}}_h^i} \int_e \{\sigma(\mathbf{v}) \mathbf{n}_e\} \cdot [\mathbf{w}] ds - \sum_{e \in \mathring{\mathcal{E}}_h^i} \int_e \{\sigma(\mathbf{w}) \mathbf{n}_e\} \cdot [\mathbf{v}] ds + \sum_{e \in \mathring{\mathcal{E}}_h^i} \frac{\rho}{h} \int_e [\mathbf{w}] \cdot [\mathbf{v}] ds. \end{aligned} \tag{5.9}$$

Denote each term on the right in (5.9) by Q_i, $i = 1, 2, \cdots, 5$. For Q_1, Q_2, the Hölder's inequality directly yields

$$|Q_1| \leqslant \sum_{T \in \mathcal{T}_h} \|\sqrt{2\mu}\epsilon(\mathbf{w})\|_{L^2(T)} \|\sqrt{2\mu}\epsilon(\mathbf{v})\|_{L^2(T)} \leqslant |||\mathbf{w}|||_h\ |||\mathbf{v}|||_h, \tag{5.10}$$

$$|Q_2| \leqslant \sum_{T \in \mathcal{T}_h} \|\sqrt{\lambda}(\nabla \cdot \mathbf{w})\|_{L^2(T)} \|\sqrt{\lambda}(\nabla \cdot \mathbf{v})\|_{L^2(T)} \leqslant |||\mathbf{w}|||_h\ |||\mathbf{v}|||_h. \tag{5.11}$$

For Q_3, Q_4 and Q_5, a similar argument yields

$$\begin{aligned} |Q_3| &\leqslant \sum_{e \in \mathring{\mathcal{E}}_h^i} \|\{\sigma(\mathbf{v})\mathbf{n}_e\}\|_{L^2(e)}\ \|[\mathbf{w}]\|_{L^2(e)} \\ &\leqslant \left(\sum_{e \in \mathring{\mathcal{E}}_h^i} \rho^{-1} \|h^{1/2}\{\sigma(\mathbf{v})\mathbf{n}_e\}\|^2_{L^2(e)} \right)^{1/2} \left(\sum_{e \in \mathring{\mathcal{E}}_h^i} \rho \|h^{-1/2}[\mathbf{w}]\|^2_{L^2(e)} \right)^{1/2} \\ &\leqslant |||\mathbf{w}|||_h |||\mathbf{v}|||_h, \end{aligned} \tag{5.12}$$

$$\begin{aligned} |Q_4| &\leqslant \sum_{e \in \mathring{\mathcal{E}}_h^i} \|\{\sigma(\mathbf{w})\mathbf{n}_e\}\|_{L^2(e)}\ \|[\mathbf{v}]\|_{L^2(e)} \\ &\leqslant \left(\sum_{e \in \mathring{\mathcal{E}}_h^i} \rho^{-1} \|h^{1/2}\{\sigma(\mathbf{w})\mathbf{n}_e\}\|^2_{L^2(e)} \right)^{1/2} \left(\sum_{e \in \mathring{\mathcal{E}}_h^i} \rho \|h^{-1/2}[\mathbf{v}]\|^2_{L^2(e)} \right)^{1/2} \\ &\leqslant |||\mathbf{w}|||_h |||\mathbf{v}|||_h, \end{aligned} \tag{5.13}$$

$$\begin{aligned} |Q_5| &\leqslant \sum_{e \in \mathring{\mathcal{E}}_h^i} \rho^{1/2} \|h^{-1/2}[\mathbf{v}]\|_{L^2(e)}\ \rho^{1/2} \|h^{-1/2}[\mathbf{w}]\|_{L^2(e)} \\ &\leqslant \left(\sum_{e \in \mathring{\mathcal{E}}_h^i} \rho \|h^{-1/2}[\mathbf{v}]\|^2_{L^2(e)} \right)^{1/2} \left(\sum_{e \in \mathring{\mathcal{E}}_h^i} \rho \|h^{1/2}[\mathbf{w}]\|^2_{L^2(e)} \right)^{1/2} \\ &\leqslant |||\mathbf{v}|||_h\ |||\mathbf{w}|||_h. \end{aligned} \tag{5.14}$$

Then, (5.8) follows form applying (5.10)-(5.14) to (5.9). □

We note that the coercivity guarantees the existence and uniqueness of the solution $\mathbf{u}_h$ determined by the PPIFE scheme (2.17). Now, we present error estimation for the IFE solution $\mathbf{u}_h$, and we first consider the error bound in the energy norm $|||\cdot|||_h$.

Theorem 5.3. *Assume $\mathbf{u} \in \mathbf{PH}^2(\Omega)$ is the exact solution to the elasticity interface problem* (1.1a)-(1.1e)*, and let $\mathbf{u}_h$ be the corresponding SPPIFE/NPPIFE/IPPIFE solution defined by* (2.17) *with ρ sufficiently large according to* (5.7) *on a Cartesian triangular or rectangular mesh $\mathcal{T}_h$ whose mesh size is sufficiently small. Then there exists a constant C such that*

$$|||\mathbf{u} - \mathbf{u}_h|||_h \leqslant Ch\|\mathbf{u}\|_{\mathbf{PH}^2(\Omega)}. \tag{5.15}$$

Proof. By (2.14) and (2.17), we have

$$a_h(\mathbf{u}_h - I_h\mathbf{u}, \mathbf{v}) = a_h(\mathbf{u} - I_h\mathbf{u}, \mathbf{v}), \quad \forall \mathbf{v} \in \mathbf{S}_h(T). \tag{5.16}$$

Let ρ be large enough such that (5.7) is satisfied. Then, letting $\mathbf{v} = \mathbf{u}_h - I_h\mathbf{u}$ in (5.16), by the coercivity (5.1) and boundedness (5.8) of the bilinear form $a_h(\cdot,\cdot)$, we have

$$\begin{aligned} \frac{1}{2}|||\mathbf{u}_h - I_h\mathbf{u}|||_h^2 &\leqslant a_h(\mathbf{u}_h - I_h\mathbf{u}, \mathbf{u}_h - I_h\mathbf{u}) = a_h(\mathbf{u} - I_h\mathbf{u}, \mathbf{u}_h - I_h\mathbf{u}) \\ &\leqslant \beta|||\mathbf{u} - I_h\mathbf{u}|||_h \, |||\mathbf{u}_h - I_h\mathbf{u}|||_h, \end{aligned} \tag{5.17}$$

which leads to $|||\mathbf{u}_h - I_h\mathbf{u}|||_h \leqslant 2\beta|||\mathbf{u} - I_h\mathbf{u}|||_h$. Hence, for the IFE solution $\mathbf{u}_h$ generated by the SPPIFE/NPPIFE/IPPIFE scheme, by the triangle inequality and estimate (4.31), we have

$$|||\mathbf{u} - \mathbf{u}_h||| \leqslant |||\mathbf{u} - I_h\mathbf{u}|||_h + |||\mathbf{u}_h - I_h\mathbf{u}|||_h \leqslant (1 + 2\beta)|||\mathbf{u} - I_h\mathbf{u}|||_h \leqslant Ch\|\mathbf{u}\|_{\mathbf{PH}^2(\Omega)},$$

which proves the error estimate (5.15). □

Next, we derive the error estimate in L^2 norm with the standard duality argument.

Theorem 5.4. *Under the condition of Theorem 5.3, there exists a constant C such that*

$$\|\mathbf{u} - \mathbf{u}_h\|_{L^2(\Omega)} \leqslant Ch^2\|\mathbf{u}\|_{\mathbf{PH}^2(\Omega)}. \tag{5.18}$$

Proof. According to the regularity of elasticity interface problem in [34], we can define an auxiliary function $\boldsymbol{\omega} = (\omega_1, \omega_2)^T \in \mathbf{PH}^2(\Omega)$ that is the solution to (1.1a)-(1.1e) with the right hand side $\mathbf{f}$ replaced by the error $\mathbf{u} - \mathbf{u}_h$. Since $\mathbf{u} - \mathbf{u}_h \in \mathbf{V}_h$, a similar derivation to (2.11) and (2.12) yields

$$\|\mathbf{u} - \mathbf{u}_h\|_{L^2(\Omega)}^2 = \int_\Omega (\text{div } \sigma(\boldsymbol{\omega})) \cdot (\mathbf{u} - \mathbf{u}_h) dX = a_h(\boldsymbol{\omega}, \mathbf{u} - \mathbf{u}_h). \tag{5.19}$$

Let $I_h\boldsymbol{\omega} \in \mathbf{S}_h(\Omega)$ be the IFE interpolation of $\boldsymbol{\omega}$. Since $a_h(I_h\boldsymbol{\omega}, \mathbf{u} - \mathbf{u}_h) = 0$, we have $a_h(\boldsymbol{\omega}, \mathbf{u} - \mathbf{u}_h) = a_h(\boldsymbol{\omega} - I_h\boldsymbol{\omega}, \mathbf{u} - \mathbf{u}_h)$. Then the boundedness of the bilinear form $a_h(\cdot,\cdot)$ leads

$$\|\mathbf{u} - \mathbf{u}_h\|_{L^2(\Omega)}^2 = a_h(\boldsymbol{\omega}, \mathbf{u} - \mathbf{u}_h) = a_h(\boldsymbol{\omega} - I_h\boldsymbol{\omega}, \mathbf{u} - \mathbf{u}_h) \leqslant \beta|||\boldsymbol{\omega} - I_h\boldsymbol{\omega}|||_h \, |||\mathbf{u} - \mathbf{u}_h|||_h. \tag{5.20}$$

In addition, since $\boldsymbol{\omega} = (\omega_1, \omega_2)^T \in \mathbf{PH}^2(\Omega)$, we can apply the estimate for the IFE interpolation (4.31) to have

$$|||\boldsymbol{\omega} - I_h\boldsymbol{\omega}|||_h \leqslant Ch\|\boldsymbol{\omega}\|_{\mathbf{PH}^2(\Omega)} \leqslant Ch\|\mathbf{u} - \mathbf{u}_h\|_{L^2(\Omega)}. \tag{5.21}$$

Finally, by applying (5.21) and Theorem 5.3 to (5.20), we have

$$\|\mathbf{u} - \mathbf{u}_h\|_{L^2(\Omega)}^2 \leqslant Ch^2\|\mathbf{u} - \mathbf{u}_h\|_{L^2(\Omega)}\|\mathbf{u}\|_{\mathbf{PH}^2(\Omega)}, \tag{5.22}$$

which leads to the estimate in (5.18). □

6 Numerical Examples

In this section, we present a group of numerical results that corroborate the error analysis presented in the previous section. In these numerical experiments, a Cartesian mesh for the domain $\Omega = [-1, 1]\times[-1, 1]$ is formed by cutting Ω into $N \times N$ squares with the mesh size $h = 2/N$. We generate the numerical results with the bilinear SPPIFE ($\theta = -1$) method using $\rho = 30 \max_{s=\pm}\{\lambda^s, \mu^s\}$ and the classic IFE method [21, 39] on a sequence of meshes, and we estimate the convergence rates of the errors computed on every two consecutive meshes in terms of the L^∞ norm, L^2 norm, and H^1 semi-norm.

In the first two numerical examples, we aim to compare the proposed PPIFE method and the classic IFE method for solving the linear elasticity interface problems. Recall from [21, 39], the classic IFE solution $\mathbf{u}_h$ is defined by the following discretized variational form:

$$\sum_{T\in\mathcal{T}_h}\left(\int_T 2\mu\epsilon(\mathbf{u}_h) : \epsilon(\mathbf{v}_h)dX + \lambda(\nabla\cdot\mathbf{u}_h)(\nabla\cdot\mathbf{v}_h)dX\right) = \sum_{T\in\mathcal{T}_h}\int_T \mathbf{f}\cdot\mathbf{v}_h dX, \quad \forall\mathbf{v}_h \in \mathbf{S}_h(\Omega). \tag{6.1}$$

We note that the proposed PPIFE method (2.15)-(2.17) is different from the classic IFE method (6.1) mainly because of those terms involving line integrals on interface edges added in (2.15) for dealing with the discontinuity of IFE functions.

Example 1: We consider a simple interface problem in which the interface is a line $\Gamma : x_1+x_2-2\pi/3 = 0$ cuts Ω into two sub-domains $\Omega^- : x_1 + x_2 - 1.5/\pi < 0$ and $\Omega^+ : x_1 + x_2 - 1.5/\pi > 0$. The exact solution is also a linear vector function given by

$$\mathbf{u}^s(X) = \begin{cases} (x_1 + x_2 - 1.5/\pi)/\lambda^s, \\ (x_1 + x_2 - 1.5/\pi)/\lambda^s, \end{cases} \quad \text{on } \Omega^s,\ s = \pm, \tag{6.2}$$

with $\lambda^- = \mu^- = 1$ and $\lambda^+ = \mu^+ = 10$, by which the boundary condition and body force in the interface problem are determined. We note that the function (6.2) is in the corresponding elasticity IFE space. Compared to the obvious errors of the classic IFE method, the SPPIFE method can produce accurate results, i.e., the SPPIFE solution is exactly the function (6.2), see the results in Tables 1 and 2. We believe this is the consequence of the consistence of the PPIFE method, i.e. if the exact solution $\mathbf{u}$ to the interface problem is such that $\mathbf{u} \in \mathbf{PH}^2(\Omega)$, then $a_h(\mathbf{u} - \mathbf{u}_h, \mathbf{v}_h) = 0$, $\forall\mathbf{v}_h \in \mathbf{S}_h(\Omega)$.

h	$\|\mathbf{u} - \mathbf{u}_h\|_{L^\infty(\Omega)}$	$\|\mathbf{u} - \mathbf{u}_h\|_{L^2(\Omega)}$	$\|\mathbf{u} - \mathbf{u}_h\|_{\mathbf{PH}^1(\Omega)}$
1/2	8.0840e-02	7.7812e-02	2.2946e-01
1/4	1.8265e-03	1.1554e-03	6.3312e-03
1/8	1.6146e-03	8.8800e-04	8.2845e-03

Table 1: Errors of classic IFE solutions for $\lambda^- = \mu^- = 1$, $\lambda^+ = \mu^+ = 10$ for Example 1.

h	$\|\mathbf{u} - \mathbf{u}_h\|_{L^\infty(\Omega)}$	$\|\mathbf{u} - \mathbf{u}_h\|_{L^2(\Omega)}$	$\|\mathbf{u} - \mathbf{u}_h\|_{\mathbf{PH}^1(\Omega)}$
1/2	4.4409e-16	4.5269e-16	8.8509e-16
1/4	3.9968e-15	3.1617e-15	1.0767e-14
1/8	1.7208e-15	1.1623e-15	5.4891e-15

Table 2: Errors of SPPIFE solutions for $\lambda^- = \mu^- = 1$, $\lambda^+ = \mu^+ = 10$ for Example 1.

Example 2: We consider a benchmark example from [46] which has been used in other articles such as [7, 28]. This example has a circular interface described by the zero level set: $x_1^2+x_2^2=a^2$ that separates the domain $\Omega=[-1,1]\times[-1,1]$ into two sub-domains $\Omega^-: x_1^2+x_2^2<a^2$ and $\Omega^+: x_1^2+x_2^2>a^2$. On Ω, the displacement is defined in the polar coordinates i.e., $\mathbf{u}=(u^r,u^\theta)^T$, where u^r and u^θ represent the radial component and circumferential component, respectively. Then the exact solution is given by $u^\theta=0$ and

$$u^r(r)=\begin{cases}\left(\left(1-\frac{b^2}{a^2}\right)c+\frac{b^2}{a^2}\right), & \text{on } \Omega^-,\\ \left(r-\frac{b^2}{r}\right)c+\frac{b^2}{r}, & \text{on } \Omega^+,\end{cases} \tag{6.3}$$

with

$$c=\frac{(\lambda^-+\mu^-+\mu^+)b^2}{(\lambda^++\mu^+)a^2+(\lambda^-+\mu^-)(b^2-a^2)+\mu^+b^2}. \tag{6.4}$$

Also, the body force in Ω and the boundary displacement on $\partial\Omega$ are generated according to (6.3). We choose $a=\pi/8$ and $b=2$ in (6.3) and (6.4), and employ the same Lamé parameters used by [7, 28, 46] in our computation: $\lambda^-=\mu^-=0.4$ in Ω^- and $\lambda^+=5.7692$, $\mu^+=3.8461$ in Ω^+, which correspond to the Young's modules $E^-=1$, $\nu^-=0.25$ and $E^+=10$, $\nu^+=0.3$.

The data in Table 3 indicates a sub-optimal convergence of the classic IFE method. Nevertheless, according to Table 4, the SPPIFE method converges optimally in both the L^2 norm and semi-H^1 norm. The data in Table 4 indicates that the convergence of the SPPIFE method in the L^∞ norm might deteriorate when the mesh becomes finer, but it is much better than the classic IFE method.

h	$\|\mathbf{u}-\mathbf{u}_h\|_{L^\infty(\Omega)}$	rate	$\|\mathbf{u}-\mathbf{u}_h\|_{L^2(\Omega)}$	rate	$\|\mathbf{u}-\mathbf{u}_h\|_{\mathbf{PH}^1(\Omega)}$	rate
1/10	8.0609E-2		4.6267E-2		6.5199E-1	
1/20	6.7026E-2	0.2662	2.0816E-2	1.1523	5.7409E-1	0.1836
1/40	5.3065E-2	0.3369	7.9983E-3	1.3799	3.9965E-1	0.5225
1/80	3.7741E-2	0.4917	3.5784E-3	1.1604	3.5914E-1	0.1542
1/160	1.7209E-2	1.1329	1.4183E-3	1.3352	2.5530E-1	0.4923
1/320	9.3939E-3	0.8734	5.5905E-4	1.3431	1.7710E-1	0.5277
1/640	5.0778E-3	0.8875	2.5381E-4	1.1393	1.3084E-1	0.4367

Table 3: Errors of the classic IFE solutions for $\lambda^-=\mu^-=0.4$, $\lambda^+=5.7692$ and $\mu^+=3.8461$ for Example 2.

h	$\|\mathbf{u}-\mathbf{u}_h\|_{L^\infty(\Omega)}$	rate	$\|\mathbf{u}-\mathbf{u}_h\|_{L^2(\Omega)}$	rate	$\|\mathbf{u}-\mathbf{u}_h\|_{\mathbf{PH}^1(\Omega)}$	rate
1/10	6.9597E-2		3.5335E-2		4.6843E-1	
1/20	2.1967E-2	1.6637	8.2012E-3	2.1072	2.1572E-1	1.1187
1/40	4.9360E-3	2.1539	2.1165E-3	1.9542	1.0506E-1	1.0379
1/80	1.7577E-3	1.4897	5.1717E-4	2.0329	5.0728E-2	1.0504
1/160	4.9811E-4	1.8191	1.1584E-4	2.1585	2.3756E-2	1.0945
1/320	1.3869E-4	1.8446	2.7700E-5	2.0642	1.1531E-2	1.0428
1/640	3.8867E-5	1.8353	6.9254E-6	1.9999	5.7069E-3	1.0147

Table 4: Errors of SPPIFE solutions for $\lambda^-=\mu^-=0.4$, $\lambda^+=5.7692$ and $\mu^+=3.8461$ for Example 2.

In summary, according to the two examples above, because those edge integral terms contribute

favorably to the accuracy of the numerical solution and the related error estimation, the proposed PPIFE method is superior to the classic IFE method in the literature [21, 39].

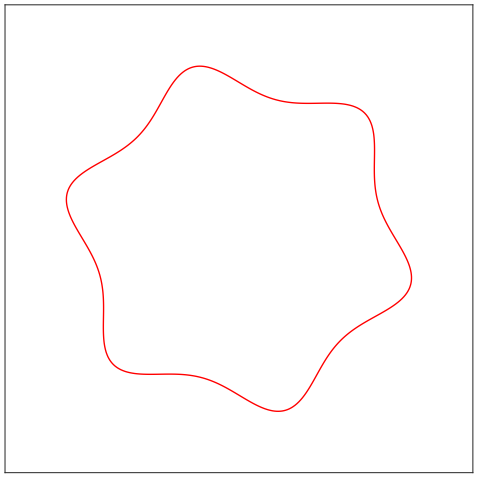

Figure 6.1: A star shape interface

Example 3: In this example, we demonstrate the performance of the proposed PPIFE method for a problem whose interface has a more sophisticated geometry. We consider an interface curve with a star shape as shown in Figure 6.1. The level set function for this curve is given by

$$S(x_1, x_2) = (x_1^2 + x_2^2)^2(1 + 0.4\sin(6\arctan(x_2/x_1)). \tag{6.5}$$

Then the interface $\Gamma : S(x_1, x_2) = 0$ partitions Ω into $\Omega^- : S(x_1, x_2) < 0$ and $\Omega^+ : S(x_1, x_2) > 0$, and the exact solution is given by

$$\mathbf{u}(x_1, x_2) = \begin{cases} \begin{bmatrix} u_1^-(x_1, x_2) \\ u_2^-(x_1, x_2) \end{bmatrix} = \begin{bmatrix} \frac{S(x_1,x_2)}{\lambda^-} \\ \frac{S(x_1,x_2)}{\lambda^-} \end{bmatrix} & \text{if } X \in \Omega^-, \\ \begin{bmatrix} u_1^+(x_1, x_2) \\ u_2^+(x_1, x_2) \end{bmatrix} = \begin{bmatrix} \frac{S(x_1,)x_2}{\lambda^+} \\ \frac{S(x_1,x_2)}{\lambda^+} \end{bmatrix} & \text{if } X \in \Omega^+. \end{cases} \tag{6.6}$$

Again, the body force and boundary displacement are generated by (6.6). In addition, we consider the Lamé parameters: $\lambda^- = \mu^- = 1$ and $\lambda^+ = \mu^+ = 1000$ which represent a fairly large difference in materials. The numerical results are presented in Table 5 which clearly demonstrate the optimal convergence for the PPIFE solutions.

h	$\|\mathbf{u}-\mathbf{u}_h\|_{L^\infty(\Omega)}$	rate	$\|\mathbf{u}-\mathbf{u}_h\|_{L^2(\Omega)}$	rate	$\|\mathbf{u}-\mathbf{u}_h\|_{\mathbf{PH}^1(\Omega)}$	rate
1/10	8.5684e-2		7.9540e-2		4.8353e-1	
1/20	3.3536e-2	1.3533	2.8597e-2	1.4758	2.7906e-1	0.7930
1/40	8.6925e-3	1.9479	6.1476e-3	2.2177	1.2137e-1	1.2012
1/80	2.0665e-3	2.0726	1.2462e-3	2.3025	5.9253e-2	1.0345
1/160	6.6198e-4	1.6423	2.9038e-4	2.1015	2.8375e-2	1.0623
1/320	1.9428e-4	1.7686	6.8241e-5	2.0892	1.3815e-2	1.0384
1/640	5.4314e-5	1.8387	1.5204e-5	2.1662	6.7626e-3	1.0306

Table 5: Errors of SPPIFE solutions for $\lambda^- = \mu^- = 1$, $\lambda^+ = \mu^+ = 1000$ for Example 3.

References

[1] Slimane Adjerid, Ruchi Guo, and Tao Lin. High degree immersed finite element spaces by a least squares method. *Int. J. Numer. Anal. Model.*, 14:604–626, 2016.

[2] Grégoire Allaire, François Jouve, and Anca-Maria Toader. Structural optimization using sensitivity analysis and a level-set method. *J. Comput. Phys.*, 194(1):363–393, 2004.

[3] Hend B. Ameur, Martin Burger, and Benjamin Hackl. Level set methods for geometric inverse problems in linear elasticity. *Inverse Problems*, 20(3):673–696, 2004.

[4] Philippe Angot and Zhilin Li. An augmented iim & preconditioning technique for jump embedded boundary conditions. *Int. J. Numer. Anal. Mod.*, 14:712–729, 2017.

[5] Ivo Babuška. The finite element method for elliptic equations with discontinuous coefficients. *Computing (Arch. Elektron. Rechnen)*, 5:207–213, 1970.

[6] Ivo Babuška and John E. Osborn. Can a finite element method perform arbitrarily badly? *Math. Comp.*, 69(230):443–462, 2000.

[7] Roland Becker, Erik Burman, and Peter Hansbo. A Nitsche extended finite element method for incompressible elasticity with discontinuous modulus of elasticity. *Comput. Methods Appl. Mech. Engrg.*, 198(41-44):3352–3360, 2009.

[8] Dietrich Braess. *Finite elements*. Cambridge University Press, Cambridge, second edition, 2001. Theory, fast solvers, and applications in solid mechanics, Translated from the 1992 German edition by Larry L. Schumaker.

[9] Erik Burman. Ghost penalty. *Comptes Rendus Mathematique*, 348(21):1217 – 1220, 2010.

[10] Erik Burman, Johnny Guzmán, Manuel A. Sánchez, and Marcus Sarkis. Robust flux error estimation of an unfitted nitsche method for high-contrast interface problems. *IMA Journal of Numerical Analysis*, page drx017, 2017.

[11] Zhiming Chen and Jun Zou. Finite element methods and their convergence for elliptic and parabolic interface problems. *Numer. Math.*, 79(2):175–202, 1998.

[12] Eric T. Chung, Yalchin Efendiev, and Shubin Fu. Generalized multiscale finite element method for elasticity equations. *GEM Int. J. Geomath.*, 5(2):225–254, 2014.

[13] Philippe G. Ciarlet. *Mathematical elasticity. Vol. I*, volume 20 of *Studies in Mathematics and its Applications*. North-Holland Publishing Co., Amsterdam, 1988. Three-dimensional elasticity.

[14] Ray. W. Clough and James L. Tocher. Finite element stiffness matrices for analysis of plate bending. In *Matrix Methods in Structual Mechanics*, pages 515–545, 1966.

[15] Bernardo Cockburn, Dominik Schötzau, and Jing Wang. Discontinuous Galerkin methods for incompressible elastic materials. *Comput. Methods Appl. Mech. Engrg.*, 195(25-28):3184–3204, 2006.

[16] John Dolbow, Nicolas Moës, and Ted Belytschko. An extended finite element method for modeling crack growth with frictional contact. *Comput. Methods Appl. Mech. Engrg.*, 190(51-52):6825–6846, 2001.

[17] Yalchin Efendiev and Thomas Y. Hou. *Multiscale finite element methods*, volume 4 of *Surveys and Tutorials in the Applied Mathematical Sciences*. Springer, New York, 2009. Theory and applications.

[18] Ruchi Guo and Tao Lin. A group of immersed finite element spaces for elliptic interface problems. *IMA J.Numer. Anal.*, 39:482–511, 2019.

[19] Ruchi Guo and Tao Lin. A higher degree immersed finite element method based on a cauchy extension. *SIAM J. Numer. Anal.*, 57:1545–1573, 2019.

[20] Ruchi Guo and Tao Lin. An immersed finite element method for elliptic interface problems in three dimensions. *arXiv:1905.10012*, 2019.

[21] Ruchi Guo, Tao Lin, and Yanping Lin. Approximation capabilities of the immersed finite element spaces for elasticity interface problems. *Numer. Methods Partial Differential Equations*, 35(3):1243–1268, 2018.

[22] Ruchi Guo, Tao Lin, and Yanping Lin. A fixed mesh method with immersed finite elements for solving interface inverse problems. *J. Sci. Comput.*, 79(1):148–175, 2018.

[23] Ruchi Guo, Tao Lin, and Yanping Lin. Recovering elastic inclusions by shape optimization methods with immersed finite elements. *submitted*, 2018.

[24] Ruchi Guo, Tao Lin, and Xu Zhang. Nonconforming immersed finite element spaces for elliptic interface problems. *Comput. Math. Appl.*, 75(6):2002 – 2016, 2018.

[25] Ruchi Guo, Tao Lin, and Qiao Zhuang. Improved error estimation for the partially penalized immersed finite element methods for elliptic interface problems. *Int. J. Numer. Anal. Model.*, 16(4):575–589, 2019.

[26] Johnny Guzmán, Manuel A. Sánchez, and Marcus Sarkis. A finite element method for high-contrast interface problems with error estimates independent of contrast. *J. Sci. Comput.*, 73(1):330–365, 2017.

[27] Anita Hansbo and Peter Hansbo. An unfitted finite element method, based on Nitsche's method, for elliptic interface problems. *Comput. Methods Appl. Mech. Engrg.*, 191(47-48):5537–5552, 2002.

[28] Anita Hansbo and Peter Hansbo. A finite element method for the simulation of strong and weak discontinuities in solid mechanics. *Comput. Methods Appl. Mech. Engrg.*, 193(33-35):3523–3540, 2004.

[29] Peter Hansbo and Mats G. Larson. Discontinuous Galerkin and the Crouzeix-Raviart element: application to elasticity. *M2AN Math. Model. Numer. Anal.*, 37(1):63–72, 2003.

[30] Xiaoming He, Tao Lin, and Yanping Lin. A bilinear immersed finite volume element method for the diffusion equation with discontinuous coefficient. *Commun. Comput. Phys.*, 6(1):185–202, 2009.

[31] Xiaoming He, Tao Lin, Yanping Lin, and Xu Zhang. Immersed finite element methods for parabolic equations with moving interface. *Numer. Methods Partial Differential Equations*, 29(2):619–646, 2013.

[32] Jan Hegemann, Alejandro Cantarero, Casey L. Richardson, and Joseph M. Teran. An explicit update scheme for inverse parameter and interface estimation of piecewise constant coefficients in linear elliptic pdes. *SIAM J. Sci. Comput.*, 35(2), 2013.

[33] Do Y. Kwak, Seungwoo Lee, and Yunkyong Hyon. A new finite element for interface problems having robin type jump. *Int. J. Numer. Anal. Mod.*, 14:532–549, 2017.

[34] D. Leguillon and E. Sanchez-Palencia. *Computation of singular solutions in elliptic problems and elasticity*. Wiley, New York, 1987.

[35] Z. Li, T. Lin, Y. Lin, and R. C. Rogers. An immersed finite element space and its approximation capability. *Numer. Methods Partial Differential Equations*, 20(3):338–367, 2004.

[36] Min Lin, Tao Lin, and Huili Zhang. Error analysis of an immersed finite element method for Euler-Bernoulli beam interface problems. *Int. J. Numer. Anal. Mod.*, 14:822–841, 2017.

[37] Tao Lin, Yanping Lin, and Xu Zhang. A method of lines based on immersed finite elements for parabolic moving interface problems. *Adv. Appl. Math. Mech.*, 5(4):548–568, 2013.

[38] Tao Lin, Yanping Lin, and Xu Zhang. Partially penalized immersed finite element methods for elliptic interface problems. *SIAM J. Numer. Anal.*, 53(2):1121–1144, 2015.

[39] Tao Lin and Xu Zhang. Linear and bilinear immersed finite elements for planar elasticity interface problems. *J. Comput. Appl. Math.*, 236(18):4681–4699, 2012.

[40] J. M. Melenk and I. Babuška. The partition of unity finite element method: basic theory and applications. *Comput. Methods Appl. Mech. Engrg.*, 139(1-4):289–314, 1996.

[41] SERGE NICAISE and ANNA-MARGARETE SÄNDIG. Transmission problems for the laplace and elasticity operators: Regularity and boundary integral formulation. *Math. Models Methods Appl. Sci.*, 09(06):855–898, 1999.

[42] Satish C. Reddy and Lloyd N. Trefethen. Stability of the method of lines. *Numer. Math.*, 62(2):235–267, 1992.

[43] Xiaofeng Ren and Juncheng Wei. On a two-dimensional elliptic problem with large exponent in nonlinearity. *Transactions of the American Mathematical Society*, 343(2):749–763, 1994.

[44] Béatrice Rivière. *Discontinuous Galerkin methods for solving elliptic and parabolic equations*, volume 35 of *Frontiers in Applied Mathematics*. Society for Industrial and Applied Mathematics (SIAM), Philadelphia, PA, 2008. Theory and implementation.

[45] Jan Sokolowski and Jean-Paul Zolésio. *Introduction to shape optimization : shape sensitivity analysis*, volume 16 of *Springer Series in Computational Mathematics*. Springer, 1992.

[46] N. Sukumar, D. L. Chopp, N. Moës, and T. Belytschko. Modeling holes and inclusions by level sets in the extended finite-element method. *Comput. Methods Appl. Mech. Engrg.*, 190(46-47):6183–6200, 2001.

[47] N. Sukumar, Z. Y. Huang, J. H. Prévost, and Z. Suo. Partition of unity enrichment for bimaterial interface cracks. *Internat. J. Numer. Methods Engrg*, 59(8):1075–1102, 2004.

[48] Michael Yu Wang, Xiaoming Wang, and Dongming Guo. A level set method for structural topology optimization. *Comput. Methods Appl. Mech. Engrg.*, 192(1):227–246, 2003.

[49] T. Warburton and J. S. Hesthaven. On the constants in *hp*-finite element trace inverse inequalities. *Comput. Methods Appl. Mech. Engrg.*, 192(25):2765–2773, 2003.

[50] Thomas P. Wihler. Locking-free adaptive discontinuous Galerkin FEM for linear elasticity problems. *Math. Comp.*, 75(255):1087–1102, 2006.

[51] Xingzhou Yang. *Immersed interface method for elasticity problems with interfaces*. PhD thesis, North Carolina State University, 2004.

[52] Xingzhou Yang, Bo Li, and Zhilin Li. The immersed interface method for elasticity problems with interfaces. *Dyn. Contin. Discrete Impuls. Syst. Ser. A Math. Anal.*, 10(5):783–808, 2003. Progress in partial differential equations (Pullman, WA, 2002).

[53] Huili Zhang, Tao Lin, and Yanping Lin. Linear and quadratic immersed finite element methods for the multi-layer porous wall model for coronary drug-eluting stents. *Int. J. Numer. Anal. Mod.*, 15:48–73, 2018.